Fluctuations and instabilities of ferromagnetic domain-wall pairs in an external magnetic field

Hans-Benjamin Braun
Department of Physics, University of California San Diego, La Jolla California 92093-0319
*and Department of Physics, Simon Fraser University, Burnaby, British Columbia, Canada V5A 1S6**
(Received 9 May 1994)

A classical continuum model of an effectively one-dimensional ferromagnet with exchange and anisotropies of hard and easy-axis type is considered. In the presence of an external magnetic field along the easy axis, the lowest-lying topological excitations are shown to be untwisted or twisted pairs of π-domain walls. The fluctuations around these structures are investigated. It is shown that the fluctuations around the twisted and untwisted domain-wall pair are governed by the same set of operators. The untwisted domain-wall pair has exactly one unstable mode and thus represents a critical nucleus for magnetization reversal in effectively one-dimensional systems. The twisted domain-wall pair is stable for small external fields but becomes unstable for large magnetic fields. The former effect is related to thermally induced coercivity reduction in elongated particles while the latter effect is related to "chopping" of twisted Bloch wall pairs in thin films. In view of a statistical mechanical theory of magnetization reversal which will be presented in a separate article, the scattering phase shifts of spin waves around these structures are calculated. The applicability of the present theory to magnetic thin films is discussed. Finally, it is noted that the static properties of the present model are equivalent to those of a nonlinear σ model with anisotropies and an external field.

I. INTRODUCTION

Macroscopic ferromagnetic samples[1,2] consist of many domains in which the magnetization is uniform and directed along one of the minima of the crystalline anisotropy. The phase boundaries between such regions are formed by domain walls (Bloch walls) in which the magnetization vector rotates continuously between different anisotropy minima. The formation of these domains is due to the long-range magnetostatic forces which tend to avoid the formation of magnetostatic charges at the sample surface. However, domain walls have locally planar symmetry and can therefore locally be described by an effectively one-dimensional model.[1,2]

A one-dimensional description is also adequate for elongated samples of mesoscopic size if the lateral sample extension is less than a domain-wall width. Such particles are widely used in magnetic recording media; e.g., Cr O_2 particles[3] are amost perfect needles with aspect ratios of up to 20:1. For this reason and in view of tremendous recent progress in sample preparation on the nanometer scale, it is therefore of particular importance to study the model of an effectively one-dimensional ferromagnet in detail.

In the following we shall focus on a description of the magnetization within a classical field theory. Such a formulation also provides the starting point for a quantum mechanical theory in the semiclassical limit.[4] The magnetization is treated as a classical vector of constant magnitude and adjacent moments interact via exchange, thus giving rise to a "stiffness" of the spin chain. The present model contains single-ion anisotropies of hard- and easy axis type which may have demagnetizing or crystalline origin. In addition it includes an external field directed along the easy axis. Without an external field, this model is also known as a "biaxial ferromagnet."

The present model has also been used to describe weakly coupled one-dimensional (1D) ferromagnetic chains.[5] In effectively 1D antiferromagnets such as TMMC,[6] it emerges as an effective model for the sublattice magnetization. The dynamic version of this model without external field and damping has been shown to be integrable[7] and reveals a surprisingly rich palette of soliton and breather[8] solutions, the solitons playing the role of domain walls.

The simplest static, topological excitation in a biaxial ferromagnet in the absence of an external field is the π-Bloch wall[9,10] (see Fig. 1) which constitutes the tran-

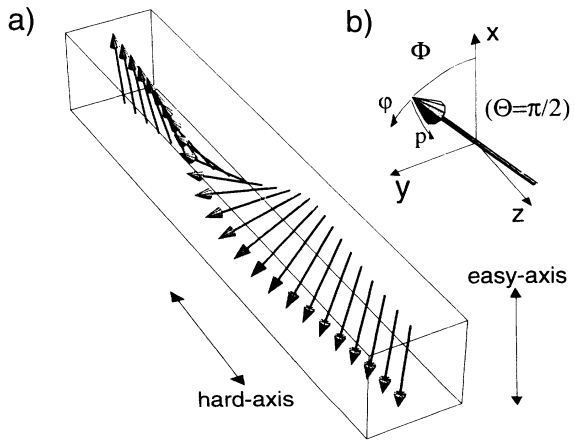

FIG. 1. (a) The π-Bloch wall interpolates between different anisotropy minima; (b) fluctuations φ, p around a given structure with ϕ_s, ϕ_b and $\theta = \pi/2$ at a given space point z.

sition region between two equivalent anisotropy minima. Its stability has been investigated by Winter[11] who explicitly derived spin-wave excitations. He showed that within the 1D system, Bloch walls are stable save for the zero energy mode which describes a rigid translation of the domain wall. Later Janak[12] quantized the spin-wave excitations around a pinned domain-wall and included demagnetizing effects of spin waves running parallel to the domain-wall. Hornreich and Thomas[13] considered a biaxial ferromagnet with an external field perpendicular to the easy axis. They studied the instability of domain-wall structures for large external fields and gave variational stability boundaries including demagnetizing effects of fluctuations.

In this paper we consider the different situation of an external field applied along the easy axis without the limitation to large external fields. The external field removes the degeneracy between the two anisotropy minima and consequently only pairs of Bloch walls can exist as static solutions. The basic topological excitations of this system are thus twisted and untwisted pairs of π-Bloch walls.

Experiments[14] and numerical simulations[15] suggest that the annihilation of twisted domain-wall pairs in thin films requires much larger external fields than that of untwisted domain-wall pairs. Furthermore, the observed[3] coercivity reduction in elongated particles at finite temperatures has no theoretical explanation.

In this work, it is shown that both of these effects are related to the stability properties of twisted and untwisted domain-wall pairs. The primary aim of the present paper is therefore a careful investigation of the fluctuations around these structures. We shall reveal the surprising fact that fluctuations around the twisted and untwisted domain-wall pairs are described by the same set of operators. This puts the stability discussion of the untwisted and twisted domain-wall pairs on an equal footing. It then follows immediately that the untwisted domain-wall pair has exactly one unstable mode corresponding to an expansion or a shrinking of the structure. The untwisted domain-wall pair is thus identified as a "nucleus" of critical size in a first-order phase transition and thus plays a crucial role in thermally activated magnetization reversal[16] in elongated particles. A detailed statistical mechanical theory of magnetization reversal is presented in the following paper.[17]

Another immediate consequence of this relation is the instability of the twisted domain-wall pair (or "2π-Bloch wall") for large external fields as has been discovered by Magyari and Thomas[18] and independently in Ref. 19. By a careful examination of the nonlocal demagnetizing fields which are not included in the model of a biaxial ferromagnet, it is shown that this effect should be observable in thin films. In particular, the minimal attainable distance of two domain walls is shown to decrease with increasing hard-axis ansiotropy. It is emphasized that this effect is beyond the otherwise highly successful description of domain walls within Slonczewski's effective model.[2] The present results are also crucial for the current design of vertical Bloch line memories[20] whose read operations rely[15] on a distinction between domain-wall pairs with different relative sense of twist.

The work is organized as follows. In Sec. II we present the model and discuss its role as an effective model which describes planar structures in a 3D model *including* demagnetizing effects. In Sec. III untwisted and twisted domain-wall pairs are presented and their energy is evaluated. It is shown that both structures can be viewed as a coherent superposition of two π-Bloch walls. In Sec. IV the operators governing the fluctuations around the 2π-Bloch wall and nucleus are derived. In Sec. V these results are applied to discuss the instabilities of these structures. In Sec. VI bound state energies and scattering phase shifts of the fluctuation operators are discussed analytically and numerically in view of a calculation of nucleation rates of magnetization reversal. The discussion of scattering phase shifts provides a lucid example of the widely unknown version of Levinson's theorem in 1D: Scattering phase shifts do not converge uniformly to those of the operators that are obtained in the limit of small and large external fields. In Sec. VII we show that the present model can account for several different experimental configurations in sufficiently thin films where the nonlocal influence of demagnetizing fields on twisted domain-wall pairs can be neglected. The present model is thus adequate to describe situations where the wall separation is comparable to the wall width.

It is not necessary that the reader follow all details of the present paper. Those who are interested in experimental implications may skip the more formal Secs. IV and VI and directly proceed to Sec. VII.

II. MODEL

In this work we consider effectively one-dimensional magnetization configurations described by the following energy per unit area:

$$\mathcal{E} = \int dz \left\{ \frac{A}{M_0^2}[(\partial_z M_x)^2 + (\partial_z M_y)^2 + (\partial_z M_z)^2] + \frac{K_h}{M_0^2} M_z^2 - \frac{K_e}{M_0^2} M_x^2 - H_{\text{ext}} M_x \right\}, \tag{2.1}$$

where $\mathbf{M} = \mathbf{M}(z)$, $\partial_z \equiv \partial/\partial z$, and $M_0 \equiv |\mathbf{M}|$ is the constant magnitude of the magnetization. The first term in the integrand of (2.1) is the classical counterpart of exchange energy and A is an exchange constant. The second term describes a hard-axis anisotropy characterized by the anisotropy constant $K_h > 0$, thus rendering the xy plane an easy plane. The rotational invariance in this easy plane is broken by an additional easy axis anisotropy with anisotropy constant $K_e > 0$. The last term in the integrand of (2.1) is the Zeeman term which is due to an external field $\mathbf{H}_{\text{ext}}$ pointing along the easy axis.

Apart from the description of the (sublattice-)spin configuration in 1D (anti)ferromagnetic systems,[5,6] the energy (2.1) has found wide applications[1,2] in the description of planar domain walls and their mobilities in bulk

ferromagnets. As will be discussed in Sec. VII, it is also adequate for the description of domain-wall pairs in thin films. Due to the absence of discussion in the recent literature, it seems convenient to review how the energy (2.1) may be derived from the energy of arbitrary 3D-magnetization configurations $\mathbf{M}=\mathbf{M}(\mathbf{r})$ in a volume V with inclusion of demagnetizing effects:

$$E=\int_V d^3r\left\{\frac{A}{M_0^2}[(\nabla M_x)^2+(\nabla M_y)^2+(\nabla M_z)^2]\right.$$
$$\left.-\frac{K_{e,\mathrm{cryst}}}{M_0^2}M_x^2+\frac{K_{h,\mathrm{cryst}}}{M_0^2}M_z^2-\frac{1}{2}\mathbf{H}_m\cdot\mathbf{M}-H_{\mathrm{ext}}M_x\right\}. \tag{2.2}$$

In contrast to (2.1), the first term in the integrand is the exchange term in three dimensions while the second and third terms describe crystalline easy- and hard-axis anisotropies of strengths $K_{e,\mathrm{cryst}}, K_{h,\mathrm{cryst}}>0$, respectively. The fourth term is the demagnetizing energy with the demagnetizing field $\mathbf{H}_m$ obeying the magnetostatic Maxwell equations $\nabla\times\mathbf{H}_m=0$, $\nabla\cdot\mathbf{B}=0$ ($\mathbf{B}=\mathbf{H}_m+4\pi\mathbf{M}$). They can be rewritten in the form of a Poisson equation $\nabla^2\Phi_m=4\pi\nabla\cdot\mathbf{M}$ with the magnetostatic potential Φ_m defined via $\mathbf{H}_m=-\nabla\Phi_m$. The Poisson equation is integrated in a standard way, and after splitting volume and surface terms we obtain

$$\mathbf{H}_m(\mathbf{r})=-\int_V d^3r'\,\rho_m(\mathbf{r}')\,\frac{\mathbf{r}-\mathbf{r}'}{|\mathbf{r}-\mathbf{r}'|^3}$$
$$+\int_{\partial V}dS'\,\sigma_m(\mathbf{r}')\,\frac{\mathbf{r}-\mathbf{r}'}{|\mathbf{r}-\mathbf{r}'|^3}, \tag{2.3}$$

where $\sigma_m(\mathbf{r})\equiv\mathbf{M}(\mathbf{r})\cdot\mathbf{n}(\mathbf{r})$ is the magnetic surface charge ($\mathbf{n}$ is the normal of the surface ∂V) and $\rho_m(\mathbf{r})=\nabla\cdot\mathbf{M}(\mathbf{r})$ is the magnetic volume charge. Inserting (2.3) into (2.2) one recognizes that the evaluation of a magnetization configuration $\mathbf{M}(\mathbf{r})$ by minimization of (2.2) for given boundary conditions is in general a hopeless task.

However, experiments reveal that the magnetization distribution in the vicinity of a domain wall in the bulk of a sample is a locally planar structure. This suggests the existence of an effective energy density which is of the form (2.1). In fact restricting ourselves to planar structures $\mathbf{M}=\mathbf{M}(z)$ and neglecting magnetic surface charges[21] in (2.3) we obtain for an infinite sample a demagnetizing field of the form

$$\mathbf{H}_m(z)=-4\pi M_z(z)\mathbf{e}_z, \tag{2.4}$$

where $\mathbf{e}_z$ is the unit vector in the z direction. For the derivation of (2.4) we have also assumed that $M_z(\pm\infty)=0$. After insertion of (2.4) into (2.2), the demagnetizing energy takes the form of a hard-axis anisotropy along the z direction. The underlying physical picture is simple: A planar arrangement of parallel dipoles has higher energy when the dipoles stick out of the plane than if they are in the plane. The form of the demagnetizing field (2.4) is used to analyze wall motion experiments in garnet films.[1] For structures of planar symmetry we thus may reduce (2.2) to (2.1) provided that

$$K_h=K_{h,\mathrm{cryst}}+2\pi M_0^2>0, \tag{2.5}$$
$$K_e=K_{e,\mathrm{cryst}}>0. \tag{2.6}$$

[This holds for a configuration as, e.g., shown in Fig. 8(a).] For other sample geometries and anisotropy configurations, we can similarly express the effective anisotropy constants K_e, K_h in (2.1) by shape and crystalline anisotropies.

To incorporate the constraint $\mathbf{M}^2=M_0^2$ =const in Eq. (2.1), we use spherical coordinates defined by $\mathbf{M}/M_0=(\sin\theta\cos\phi,\ \sin\theta\sin\phi,\ \cos\theta)$. Further it is convenient to introduce dimensionless quantities by taking the scales of length and energy per area as

$$[x]=[y]=[z]=\sqrt{\frac{A}{K_e}},\qquad [\mathcal{E}]=2\sqrt{AK_e}. \tag{2.7}$$

Consequently, the units of the magnetic field are given by $[H]=\sqrt{2K_e}$. The length $\sqrt{A/K_e}$ is the width of the static π-Bloch wall, and $2\sqrt{AK_e}$ is half the energy per unit area of the static π-Bloch wall. With these definitions, the energy (2.1) becomes

$$\mathcal{E}=\int_{-\infty}^{\infty}dz\left\{\frac{1}{2}[(\partial_z\theta)^2+\sin^2\theta(\partial_z\phi)^2]\right.$$
$$\left.-\frac{1}{2}[\sin^2\theta\cos^2\phi-1]+\frac{Q^{-1}}{2}\cos^2\theta-h\sin\theta\cos\phi\right\}, \tag{2.8}$$

where $\theta=\theta(z)$ and $\phi=\phi(z)$. The normalization is chosen such that the uniform states $\theta=\pi/2$ and $\phi=0$ or $\phi=\pi$ have zero energy in the absence of an external field. In (2.8) we have introduced the dimensionless anisotropy ratio $Q>0$ with

$$Q=\frac{K_e}{K_h}, \tag{2.9}$$

describing the ratio of easy- and hard-axis anisotropy in the effective model (2.1). Note that this is a slight extension of the common definition where $K_h=2\pi M_0^2$. In (2.8) we have also used the reduced external field h which is related to the external field H_{ext} in laboratory units by

$$h=\frac{H_{\mathrm{ext}}M_0}{2K_e}>0. \tag{2.10}$$

At first sight, the choice of the coordinate frame in (2.1) and (2.8) might be surprising since the polar angle is not measured relative to the external field. The advantage of such an orientation is that the linearization in the angles θ and ϕ around structures confined to the xy plane is equivalent to a linearization in a Cartesian frame that is rotated along this structure[11,12] but is simpler in practice. Measuring θ from the external field would not allow linearization in the azimuthal angle ϕ to describe spin-wave excitations of a uniform state parallel to the external field.

III. DOMAIN-WALL STRUCTURES

In the following we shall focus on static easy-plane structures of the model (2.8). It is shown that the only solitary easy-plane structures are twisted and untwisted pairs of π-Bloch walls. Simple representations are presented that relate these solutions to each other.

Inspecting (2.8), we recognize that the hard-axis anisotropy is minimized for $\theta = \pi/2$. The corresponding static structures then identically satisfy the Euler-Lagrange equation $\delta\mathcal{E}/\delta\theta = 0$ while the Euler-Lagrange equation in ϕ reads

$$-\frac{d^2\phi}{dz^2} + \sin\phi\cos\phi + h\sin\phi = 0. \tag{3.1}$$

Upon integration with $d\phi/dz$ we obtain the first integral

$$\frac{1}{2}\left(\frac{d\phi}{dz}\right)^2 + V(\phi) = C, \tag{3.2}$$

with

$$V(\phi) = \frac{1}{2}\cos^2\phi + h\cos\phi. \tag{3.3}$$

Equation (3.2) has the form of an energy conservation for a fictitious particle moving in the one-dimensional potential $V(\phi)$. By this analogy, we can gain an overview[19] of all static easy-plane structures. Note that the potential $V(\phi)$ is the negative of anisotropy and external field contributions to $\mathcal{E}$ for $\theta = \pi/2$ up to an irrelevant constant.

Solitary solutions are now obtained as trajectories of the fictitious particle starting from a local maximum of $V(\phi)$. Due to the "energy conservation" (3.2) it will either creep into a different maximum of the same height or, if it started from a lower maximum, it will bounce back into the same state. For $h \neq 0$ the degeneracy between the maxima of V (i.e., minima of $\mathcal{E}$) is lifted and two distinct trajectories emerge. One trajectory connects a global maximum of V at $\phi = 0$ with an adjacent one at $\phi = \pm 2\pi$. This trajectory corresponds to a twisted pair of π-Bloch walls. The second possible trajectory represents a localized excursion from the lower maximum of V at $\phi = \pm\pi$ which corresponds to an untwisted pair of π-Bloch walls. For other values of C in (3.2), periodic solutions[19] occur which may be regarded as generalizations of the above solutions to finite sample lengths.

Thus we have obtained an overview over all possible solutions without having solved the differential equation (3.2) in detail. This analog should also prove useful for different models with other forms of the anisotropy and different orientations of the external field.

Apart from the trivial symmetry arising from the representation of $\mathbf{M}$ in terms of spherical coordinates, Eq. (3.1) is invariant under the symmetry operations

$$\mathcal{R}_x(\pi) : \phi \mapsto -\phi \tag{3.4}$$

and

$$\mathcal{T} : \mathbf{M} \mapsto -\mathbf{M}, \qquad h \mapsto -h. \tag{3.5}$$

$\mathcal{R}_x(\pi)$ corresponds to an (internal) rotation of the magnetization by an angle π around the x axis ($\theta = \pi/2$), whereas $\mathcal{T}$ represents a time inversion. Therefore, all specific solutions quoted below have equivalents arising through the action of $\mathcal{R}_x$, $\mathcal{T}$, and $\mathcal{T} \circ \mathcal{R}_x$. For a given direction of the external field there are thus exactly two equivalent structures related to each other by the action of $\mathcal{R}_x(\pi)$. To classify the solutions it is also convenient to introduce the twist

$$q(\phi) = \frac{1}{2\pi}\int_{-\infty}^{\infty} dz\,\frac{d\phi}{dz}. \tag{3.6}$$

Single π-domain walls belong to $|q| = 1/2$, whereas twisted domain-wall pairs have $|q| = 1$ and untwisted pairs have $q = 0$. Note that $\mathcal{R}_x(\pi)$ changes the sign of the twist q, whereas $\mathcal{T}$ leaves the twist invariant but reverses the magnetization at infinity.

For a vanishing external field, $h = 0$, (3.2) with (3.3) may easily be integrated with the boundary conditions $\partial_z\phi(\pm\infty) = 0$, $\phi(-\infty) = 0$, and $\phi(\infty) = \pi$ to yield the π-Bloch wall

$$\phi_K(z) = 2\arctan e^z, \qquad \theta_K = \pi/2. \tag{3.7}$$

The configuration (3.7) is shown in Fig. 1. The Bloch wall represents a smooth transition region between the two degenerate uniform states of minimal anisotropy energy while the magnetization always lies in the easy plane. In (3.7) an integration constant describing the arbitrary wall position has been fixed such that the π-Bloch wall is centered around the origin. However, as we shall see in Sec. IV, this degeneracy with respect to translations will lead to a (Goldstone) mode of zero energy in the excitation spectrum. The finite domain-wall width arises through the balance of exchange energy and uniaxial anisotropy, the former tending to enlarge the transition region, the latter tending to narrow the Bloch wall.

Inserting (3.7) into (2.8) for $h = 0$ we obtain for the energy per unit area of the π-Bloch wall

$$\mathcal{E}_K = \int_{-\infty}^{\infty} dz\left(\frac{d\phi_K}{dz}\right)^2 = 2, \tag{3.8}$$

where in the first step we have made use of the fact that ϕ_K obeys the "energy conservation" (3.2) with $C = 1/2$ and $h = 0$.

For $h \neq 0$, the degeneracy between the two anisotropy minima at $(\theta, \phi) = (\pi/2, \pi)$ and $(\pi/2, 0)$ is lifted. Consequently, single Bloch walls cannot exist any more. Instead two different types of Bloch wall pairs arise which are discussed in the next two subsections.

A. Untwisted domain-wall pairs

For $0 < h < 1$, the boundary conditions $\partial_z\phi(\pm\infty) = 0$, $\phi(\pm\infty) = \pi$, imply that $C = 1/2 - h$. The integration of (3.2) then yields the "nucleus"[16,23]

$$\phi_s(z) = 2\arctan\left(\frac{\cosh z/\delta_s}{\sinh R_s}\right), \qquad \theta_s = \pi/2. \tag{3.9}$$

As we shall see in Sec. V, the configuration (3.9) represents a *saddle point* of the energy since it is unstable for all values $0 < h < 1$ of the external field. Since it has exactly one unstable mode, it represents a critical nucleus for magnetization reversal. The integration constant in (3.9) is chosen such that the symmetry center is located at $z = 0$. Note, however, that the continuous degeneracy of (3.9) with respect to translations will give rise to a zero energy (Goldstone) mode in the fluctuation spectrum, quite analogous to the case of the π-Bloch wall above. In (3.9) we have introduced the "radius" R_s of the untwisted domain-wall pair. R_s is related to the external field h and the width δ_s as follows:

$$h = \operatorname{sech}^2 R_s, \qquad \delta_s = \coth R_s. \tag{3.10}$$

The nucleus may also be written as a superposition of two *untwisted* π-Bloch walls (3.8) centered at $z/\delta_s = \pm R_s$,

$$\phi_s(z) = \phi_K(z/\delta_s - R_s) + \phi_K(-z/\delta_s - R_s). \tag{3.11}$$

Note that this relation is exact for all $0 < R_s < \infty$. Equations (3.9), (3.11) thus describe a domain with magnetization oriented parallel to the external field which is delimited by a pair of untwisted π-Bloch walls (cf. Fig. 2). The existence of this structure is due to the balance of exchange and Zeeman energy. The exchange energy tends to attract the untwisted domain walls, whereas the Zeeman energy pulls them apart since it favors the intermediate domain. As is illustrated by (3.10), (3.11), and Fig. 2, the domain-wall separation tends to infinity for $h \to 0$ whereas for $h \to 1$ the two oppositely twisted domain walls almost annihilate each other and the nucleus degenerates to an infinitesimal deviation from the uniform "down" state $(\phi, \theta) = (\pi, \pi/2)$.

Using the parametrization (3.10), the energy per unit area (2.8) of the nucleus relative to the "down" state takes the simple form

$$\mathcal{E}_s \equiv \mathcal{E}[\phi_s, \theta_s] - \mathcal{E}\left[\phi = \pi, \theta = \frac{\pi}{2}\right] = \int_{-\infty}^{\infty} dz \left(\frac{d\phi_s}{dz}\right)^2 = 4\tanh R_s - 4R_s \operatorname{sech}^2 R_s. \tag{3.12}$$

In the first step we have used the first integral (3.2) and the integration is most easily performed with (3.11). The first term on the right-hand side (rhs) in (3.12) describes the deformation energy of the nucleus compared to the uniform state in the absence of an external field. The second term is the Zeeman energy $-\mathcal{M}_s h$. The magnetic moment per unit area relative to the down state is thus given by

$$\mathcal{M}_s = 4R_s. \tag{3.13}$$

The deformation energy vanishes for $R_s \to 0$, reflecting the fact that untwisted pairs of domain walls are attractive. For $R_s \to \infty$, the energy converges to that of two independent π-Bloch walls.

From (3.12) and (3.10) we may immediately derive the (formal) susceptibility

$$\chi_s \equiv \frac{d\mathcal{M}_s}{dh} = \frac{2}{h\sqrt{1-h}}. \tag{3.14}$$

This susceptibility has only formal character, since as we shall see below, the nucleus is unstable for all values of the external field $0 < h < 1$.

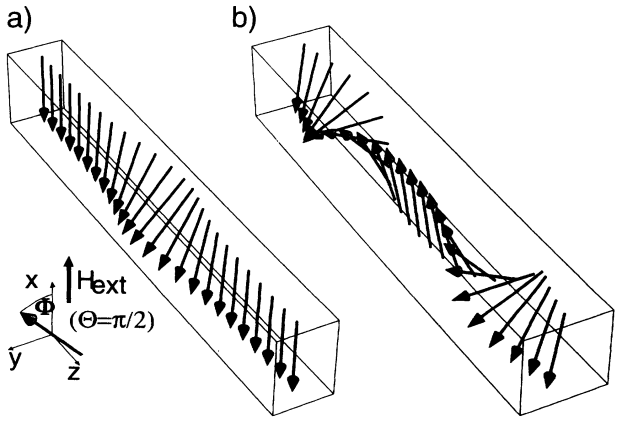

FIG. 2. The nucleus is shown for (a) small fields ($R_s = 3.5$) and (b) for fields close to the anisotropy field ($R_s = 0.4$)

B. Twisted domain-wall pairs

For $0 < h < \infty$, and for the boundary conditions $\partial_z\phi(\pm\infty) = 0$, $\phi(\pm\infty) = 0$, we have $C = 1/2 + h$. Equation (3.2) may then be integrated to yield the 2π-Bloch wall[18,19,22]

$$\phi_b(z) = 2\arctan\left(\frac{\cosh R_b}{\sinh z/\delta_b}\right), \qquad \theta_b = \pi/2. \tag{3.15}$$

The integration constant has been chosen such that the symmetry center is located at $z = 0$ but as in the case of the nucleus, the translational degeneracy will give rise to a zero energy (Goldstone) mode in the fluctuation spectrum. The "radius" R_b of the twisted domain-wall pair is related to the external field h and the characteristic width δ_b as follows:

$$h = \operatorname{csch}^2 R_b, \qquad \delta_b = \tanh R_b. \tag{3.16}$$

The 2π-Bloch wall (3.16) may also be written as a superposition of two *twisted* π-Bloch walls (3.7) located at $z/\delta_b = \pm R_b$,

$$\phi_b(z) = \phi_K(-z/\delta_b + R_b) + \phi_K(-z/\delta_b - R_b). \tag{3.17}$$

This relation is valid for all values of R_b. Equations (3.16), (3.17) describe a pair of π-Bloch walls located at $z/\delta = \pm R_b$ with equal relative sense of twist, enclosing a domain of reversed magnetization (cf. Fig. 3). This structure is stabilized by the balance of Zeeman and exchange energy. The Zeeman energy tends to enlarge the domains oriented parallel to the external field, whereas the exchange energy pulls the twisted domain walls apart. As illustrated by Fig. 3(b), the 2π-Bloch wall decays for $h \to 0$ into two individual π-Bloch walls with increasing separation, whereas for $h \to \infty$ [Fig. 3(a)], the two π-Bloch walls are squeezed and the transition region becomes infinitesimally small.

The energy per area of the 2π-Bloch wall is given by

$$\mathcal{E}_b \equiv \mathcal{E}\left[\phi_b, \theta = \frac{\pi}{2}\right] - \mathcal{E}\left[\phi = 0, \theta = \frac{\pi}{2}\right] = \int_{-\infty}^{\infty} dz \left(\frac{d\phi_b}{dz}\right)^2 = 4 \coth R_b + 4 R_b \operatorname{csch}^2 R_b. \tag{3.18}$$

where (3.2) and (3.17) have been used. The first and second terms on the rhs in (3.18) describe the deformation energy of the 2π-Bloch wall relative to the uniform "up" state $\phi = 0$ in the absence of an external field, and the Zeeman energy, respectively. The magnetic moment per unit area relative to the up state is thus given by

$$\mathcal{M}_b = -4R_b. \tag{3.19}$$

Note that the deformation energy in (3.18) diverges for $R_b \to 0$ (i.e., $h \to \infty$); i.e., a compression of the 2π-Bloch wall to zero width is connected with an infinite increase in exchange energy. For $R_b \to \infty$ (i.e., $h \to 0$) the deformation energy tends to that of two single π-Bloch walls and the Zeeman energy becomes zero. With (3.18) and (3.19) we obtain the susceptibility

$$\chi_b \equiv \frac{d\mathcal{M}_b}{dh} = \frac{2}{h\sqrt{1+h}}. \tag{3.20}$$

For large external fields this susceptibility has a only formal meaning, since the 2π-Bloch wall can become unstable for $h \gtrsim Q^{-1}/3$ as we shall see in Sec. V.

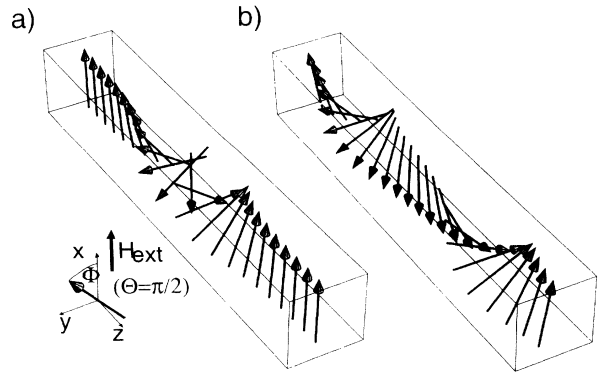

FIG. 3. The 2π-Bloch wall is shown for (a) small fields ($R_b = 3.5$) and (b) for large fields ($R_b = 0.4$)

IV. FLUCTUATIONS

To investigate the stability of the structures presented in the last section, we perform an expansion around a given easy-plane configuration $(\phi_0(z), \theta = \pi/2)$ as follows:

$$\phi(z) = \phi_0(z) + \varphi(z), \qquad \theta(z) = \pi/2 - p(z), \tag{4.1}$$

where $|\varphi|, |p| \ll 1$. First, we shall review the fluctuations around the π-Bloch wall because of their close relation to the fluctuations of the 2π-Bloch wall and the nucleus.

Inserting (4.2) with $\phi_0 = \phi_K$ into (2.8) for $h = 0$ we obtain up to second order in $\varphi(z)$ and $p(z)$

$$\mathcal{E}^{(2)} = \mathcal{E}^K + \frac{1}{2}\int_{-\infty}^{\infty} dz\, \varphi\, \mathcal{H}^K \varphi + \frac{1}{2}\int_{-\infty}^{\infty} dz\, p\, (\mathcal{H}^K + Q^{-1}) p, \tag{4.2}$$

where $\mathcal{E}^K$ is the Bloch wall energy (3.8). No first-order term in the fluctuations is present in (4.2) since ϕ_K obeys the Euler-Lagrange equations (3.1) with $h = 0$. The operator $\mathcal{H}^K$ is defined as

$$\mathcal{H}^K = -\frac{d^2}{dz^2} + 1 - 2\operatorname{sech}^2 z. \tag{4.3}$$

The potential appearing in (4.3) belongs to the family of reflectionless potentials which are of the form $-m(m+1)\operatorname{sech}^2 z$ (m an integer), and which are discussed in the Appendix. The eigenvalue problem of (4.3) is

$$\mathcal{H}^K \chi_\nu^K(z) = E_\nu^K \chi_\nu^K(z), \qquad \nu = 0, k. \tag{4.4}$$

There is one bound state with zero energy,

$$\chi_0^K(z) = \frac{1}{\sqrt{2}} \operatorname{sech} z, \quad E_0^K = 0, \tag{4.5}$$

and there are running (spin-wave) states,

$$\chi_k^K(z) = \frac{1}{\sqrt{2\pi(1+k^2)}} [-ik + \tanh z]\, e^{ikz}, \qquad E_k^K = 1 + k^2. \tag{4.6}$$

The easy-axis anisotropy leads to the gap 1 in the spin-wave spectrum (4.6) while (4.2) shows that the hard-axis anisotropy gives rise to the "mass" Q^{-1} of the p fluctuations. Since χ_0^K is nodeless and thus represents the ground state of $\mathcal{H}_K$ with eigenvalues zero, all eigenvalues of $\mathcal{H}_K + Q^{-1}$ are positive. Therefore all fluctuations around a π-Bloch wall have positive energy except for the zero energy mode $(\varphi, p) = (\chi_0^K(z), 0)$. This mode corresponds to a rigid translation of the Bloch wall: Taking the derivative of (3.2) for $h = 0$ we obtain $\mathcal{H}^K d\phi_K/dz = 0$ and therefore $\chi_0^K \propto d\phi_K/dz$. We conclude that in the absence of an external field the static kink is stable with respect to planar distortions except for rigid translations

which involve zero energy. This result was first obtained by Winter.[11] We now proceed with a discussion of fluctuations of the nucleus and the 2π-Bloch wall.

A. Nucleus

Inserting (4.1) with $\phi_0 = \phi_s$ into the energy (2.8) and evaluating $\mathcal{E}[\phi,\theta] - \mathcal{E}[\phi = \pi, \theta = \frac{\pi}{2}]$ to second order in φ and p we obtain

$$\mathcal{E}_s^{(2)} \equiv \mathcal{E}_s + \frac{1}{2}\int_{-\infty}^{\infty} dz\, \varphi \mathcal{H}^{s\varphi}\varphi + \frac{1}{2}\int_{-\infty}^{\infty} dz\, p\mathcal{H}^{sp}p, \quad (4.7)$$

where $\mathcal{E}_s$ is given by (3.12). The first-order term in the fluctuations is absent since ϕ_s satisfies the Euler-Lagrange equations (3.1). The operators $\mathcal{H}^{s\varphi}$ and $\mathcal{H}^{sp}$ are defined as

$$\mathcal{H}^{s\varphi} = -\frac{d^2}{dz^2} + 2\cos^2\phi_s + \operatorname{sech}^2 R_s \cos\phi_s - 1, \quad (4.8)$$

$$\mathcal{H}^{sp} = -\frac{d^2}{dz^2} + 2\cos^2\phi_s + 3\operatorname{sech}^2 R_s \cos\phi_s + 2\operatorname{sech}^2 R_s - 1 + Q^{-1}, \quad (4.9)$$

with

$$\cos\phi_s = \frac{\sinh^2 R_s - \cosh^2(z/\delta_s)}{\sinh^2 R_s + \cosh^2(z/\delta_s)}. \quad (4.10)$$

This form of the fluctuation operators is rather involved. Since the nucleus can be represented as a superposition (3.11) of untwisted π-Bloch walls, we expect these operators to contain potentials of the form (4.3) for each of the constituents of the nucleus. Indeed, (4.8) and (4.9) allow for the much simpler representation

$$\mathcal{H}^{s\varphi} = -\frac{d^2}{dz^2} + \delta_s^{-2} V_-\left(\frac{z}{\delta_s}, R_s\right), \quad (4.11)$$

$$\mathcal{H}^{sp} = -\frac{d^2}{dz^2} + \delta_s^{-2} V_+\left(\frac{z}{\delta_s}, R_s\right) + Q^{-1}, \quad (4.12)$$

where the potentials $V_\pm$ are given by

$$V_\pm(\zeta, R) = 1 - 2\operatorname{sech}^2(\zeta + R) - 2\operatorname{sech}^2(\zeta - R) \pm 2\operatorname{sech}(\zeta + R)\operatorname{sech}(\zeta - R). \quad (4.13)$$

The second and third terms on the rhs of (4.13) are the potentials (4.3) of two noninteracting π-Bloch walls located at $z/\delta_b = \pm R_b$. The last term, which vanishes for $R_s \to \infty$, describes the interaction of the two π-Bloch walls and is thus sensitive to their relative sense of twist. The constant Q^{-1} in (4.12) is due to the hard-axis anisotropy and leads, in analogy to the π-Bloch wall, to a finite mass of fluctuations out of the easy plane. The corresponding eigenvalue problems are

$$\mathcal{H}^{s\varphi}\chi_\nu^{s\varphi}(z, R_s) = E_\nu^{s\varphi}(R_s)\chi_\nu^{s\varphi}(z, R_s), \quad (4.14)$$

$$\mathcal{H}^{sp}\chi_\nu^{sp}(z, R_s) = E_\nu^{sp}(R_s)\chi_\nu^{sp}(z, R_s), \quad (4.15)$$

where the index ν denotes bound states and scattering states. An analytical solution of these eigenvalue problems seems only possible in the limiting cases $R_s \to 0$ and $R_s \to \infty$. However, one bound state of $\mathcal{H}^{s\varphi}$, the zero energy state, can be derived immediately by taking advantage of the continuous degeneracy of (2) with respect to translations. Taking the z derivative of (3.1) at $\phi = \phi_s$, we obtain with (4.8) $\mathcal{H}^{s\varphi} d\phi_s/dz = 0$, and therefore

$$\chi_1^{s\varphi} \propto \frac{d\phi_s}{dz} = \delta_s^{-1}\left\{\operatorname{sech}\left(\frac{z}{\delta_s} + R_s\right) - \operatorname{sech}\left(\frac{z}{\delta_s} - R_s\right)\right\}, \quad (4.16)$$

$$E_1^{s\varphi} = 0.$$

The antisymmetry of the zero mode $\chi_1^{s\varphi}$ with respect to z is a consequence of the opposite relative sense of twist of the two π-Bloch walls in (3.11). The remaining bound state energies and the scattering phase shifts will be investigated analytically and numerically in the next section.

B. 2π-Bloch wall

Inserting (4.1) with $\phi_0 = \phi_b$ into (2.8) we obtain for $\mathcal{E}[\phi,\theta] - \mathcal{E}[\phi = 0, \theta = \frac{\pi}{2}]$ to second order in φ and p

$$\mathcal{E}_b^{(2)} \equiv \mathcal{E}_b + \frac{1}{2}\int_{-\infty}^{\infty} dz\, \varphi \mathcal{H}^{b\varphi}\varphi + \frac{1}{2}\int_{-\infty}^{\infty} dz\, p\mathcal{H}^{bp}p, \quad (4.17)$$

with $\mathcal{E}_b$ given by (3.18). The operators $\mathcal{H}^{b\varphi}$ and $\mathcal{H}^{bp}$ are defined as

$$\mathcal{H}^{b\varphi} = -\frac{d^2}{dz^2} + 2\cos^2\phi_b + \operatorname{csch}^2 R_b \cos\phi_b - 1, \quad (4.18)$$

$$\mathcal{H}^{bp} = -\frac{d^2}{dz^2} + 2\cos^2\phi_b + 3\operatorname{csch}^2 R_b \cos\phi_b - 2\operatorname{csch}^2 R_b - 1 + Q^{-1}, \quad (4.19)$$

with

$$\cos\phi_b = \frac{\sinh^2(z/\delta_b) - \cosh^2 R_b}{\sinh^2(z/\delta_b) + \cosh^2 R_b}. \quad (4.20)$$

The operator (4.18) is identical to that describing the fluctuations around a kink in the double sine-Gordon model.[24] In analogy to the nucleus, (4.18) and (4.19) allow for a much simpler representation

$$\mathcal{H}^{b\varphi} = -\frac{d^2}{dz^2} + \delta_b^{-2} V_+\left(\frac{z}{\delta_b}, R_b\right), \quad (4.21)$$

$$\mathcal{H}^{bp} = -\frac{d^2}{dz^2} + \delta_b^{-2} V_-\left(\frac{z}{\delta_b}, R_b\right) + Q^{-1}, \quad (4.22)$$

where the potentials $V_\pm$ are given by (4.13). The representation (4.21) has also been obtained by Sodano *et al.*[25] in the discussion of kinks in the double sine-Gordon model. It is instructive to compare (4.21) and (4.22) with (4.3): The second and third terms on the rhs of (4.13) are the potentials of the noninteracting domain walls located at $z/\delta_b = \pm R_b$. The last term describes the interaction of the two domain walls and vanishes for $R_b \to \infty$. The constant Q^{-1} in (4.22) is due to the hard-axis anisotropy and leads to a finite mass of out of easy-plane fluctuations.

We write the eigenvalue problem of (4.21) and (4.22) in the following form:

$$\mathcal{H}^{b\varphi}\chi_\nu^{b\varphi}(z,R_b) = E_\nu^{b\varphi}(R_b)\chi_\nu^{b\varphi}(z,R_b), \tag{4.23}$$

$$\mathcal{H}^{bp}\chi_\nu^{bp}(z,R_b) = E_\nu^{bp}(R_b)\chi_\nu^{bp}(z,R_b). \tag{4.24}$$

The index ν denotes bound states and scattering states. Again, an analytic solution of these eigenvalue problems seems only possible in the limiting cases $R_s \to 0$ and $R_s \to \infty$. In analogy to the nucleus, one bound state of $\mathcal{H}^{s\varphi}$ can be derived immediately. Taking the z derivative of (3.1) at $\phi = \phi_s$ we obtain $\mathcal{H}^{s\varphi}d\phi_s/dz = 0$ and therefore

$$\chi_0^{b\varphi} \propto \frac{d\phi_b}{dz} = \delta_b^{-1}\left\{\operatorname{sech}\left(\frac{z}{\delta_b}+R_b\right)+\operatorname{sech}\left(\frac{z}{\delta_b}-R_b\right)\right\}, \tag{4.25}$$

$$E_0^{b\varphi} = 0.$$

The symmetry of $\chi_0^{b\varphi}$ with respect to z reflects the equal sense of twist of the two domain walls in (3.16).

V. INSTABILITIES

We are now in a position to state one of the central results of this paper. Comparing (4.21), (4.22) with (4.11) and (4.12) we infer the remarkable connection

$$\mathcal{H}^{sp}(z,R) = \left(\frac{\delta_b}{\delta_s}\right)^2 \mathcal{H}^{b\varphi}\left(\frac{\delta_b}{\delta_s}z,R\right) + Q^{-1}, \tag{5.1}$$

$$\mathcal{H}^{bp}(z,R) = \left(\frac{\delta_s}{\delta_b}\right)^2 \mathcal{H}^{s\varphi}\left(\frac{\delta_s}{\delta_b}z,R\right) + Q^{-1}. \tag{5.2}$$

Here, for clarity, the notation $\mathcal{H}^{s\varphi}(z,R) \equiv -d^2/dz^2 + \delta_s^{-2}V_-(\frac{z}{\delta_s},R)$, $\delta_s = \coth R$, has been used and analogously for the remaining operators. Equations (5.1), (5.2) show that the fluctuations around the 2π-Bloch wall and around the nucleus are governed up to rescaling by the same set of operators. Consequently the eigenvalues are related by

$$E_\nu^{sp}(R) = \left(\frac{\delta_b}{\delta_s}\right)^2 E_{\nu'}^{b\varphi}(R) + Q^{-1}, \tag{5.3}$$

$$E_{\nu'}^{bp}(R) = \left(\frac{\delta_s}{\delta_b}\right)^2 E_\nu^{s\varphi}(R) + Q^{-1}, \tag{5.4}$$

and the eigenfunctions obey

$$\chi_\nu^{sp}(z,R) = \chi_{\nu'}^{b\varphi}\left(\frac{\delta_b}{\delta_s}z,R\right), \tag{5.5}$$

$$\chi_{\nu'}^{bp}(z,R) = \chi_\nu^{s\varphi}\left(\frac{\delta_s}{\delta_b}z,R\right), \tag{5.6}$$

where for bound states $\nu = \nu'$ and for scattering states $\nu = k$, $\nu' = (\delta_s/\delta_b)k$. The continuum eigenvalues are defined as $E_k^{j\varphi} = \delta_j^{-2} + k^2$, $E_k^{jp} = Q^{-1} + E_k^{j\varphi}$ for $j = s, b$. In (5.1)–(5.6) we have used

$$\delta_b/\delta_s = \tanh^2 R. \tag{5.7}$$

The relations (5.3), (5.4) together with (4.16), (4.25) now allow us to discuss instabilities of the nucleus and the 2π-Bloch wall in a simple and straightforward way.

The function $\chi_0^{b\varphi}$ as given in (4.25) is symmetric and nodeless, and hence it represents the ground state of $\mathcal{H}^{b\varphi}$ with zero energy. Except for this state, $\mathcal{H}^{b\varphi}$ has a strictly positive spectrum and so has $\mathcal{H}^{sp}$, i.e.,

$$E_\nu^{b\varphi}(R_b) \geq 0, \quad E_\mu^{sp}(R_s) > 0, \tag{5.8}$$

for all ν and $0 < R_b, R_s < \infty$. It thus follows that (i) the 2π-Bloch wall is stable with respect to easy-plane fluctuations (neutrally stable with respect to the zero mode), and (ii) that the nucleus is stable with respect to out of easy-plane fluctuations.

On the other hand, the function $\chi_1^{s\varphi}$ is antisymmetric with one node and thus represents the first excited state of $\mathcal{H}^{s\varphi}$. Since it has zero energy, there is exactly one nodeless, symmetric bound state of *negative* energy, i.e.,

$$E_0^{s\varphi}(R_s) < 0, \tag{5.9}$$

for all $0 < R_s < \infty$. The inequality (5.9) is the origin of the following instabilities:

Nucleus: Fluctuations in φ direction exhibit exactly one mode of negative energy $E_0^{s\varphi}$. Since $\mathcal{H}^{sp}$ is positive, we conclude that *there is exactly one unstable mode of the nucleus for all values of* R_s. Since ϕ_s is untwisted [i.e., $q(\phi_s) = 0$], the instability in φ provides an example of a topologically induced instability.

2π-Bloch wall: The 2π-Bloch wall is stable with respect to φ fluctuations because of (5.8). Since $q(\phi_b) = 1$, this stability is of topological origin. However, *an instability against out of easy-plane distortions occurs if*

$$E_0^{bp}(R_b) \equiv Q^{-1} - \coth^4 R_b |E_0^{s\varphi}(R_b)| < 0, \tag{5.10}$$

where R_b is related to the external field as $h = \operatorname{csch}^2 R_b$. In (5.10) we have made use of (5.4).

Anticipating results of the next section for the asymptotic behavior of the eigenvalues, we obtain the following asymptotic behavior for this instability condition:

$$Q^{-1} < 2h, \quad h \ll 1, \tag{5.11}$$

$$Q^{-1} < 3h, \quad h \gg 1. \tag{5.12}$$

This asymptotic behavior is shown together with (5.10) in Fig. 4. The instability of the 2π-Bloch wall is in accordance with the result of Magyari and Thomas[18] who gave also an improved analytical estimate of the insta-

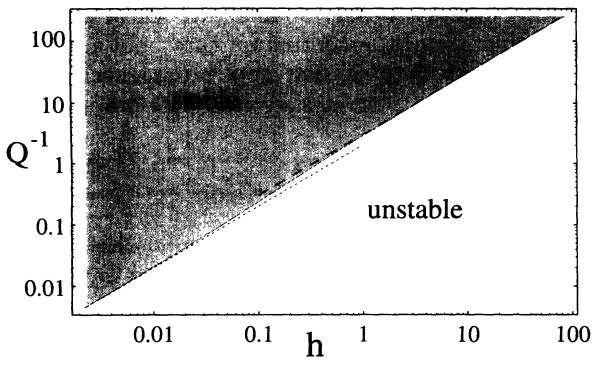

FIG. 4. Stability and instability regions of the 2π-Bloch wall as a function of the external field h and the demagnetizing field strength Q^{-1}. The dotted and dashed lines refer to (5.11) and (5.12), respectively.

bility range for large h; however, they did not discuss the nucleus and the relation of its fluctuations to the 2π-Bloch wall.

Since we have shown in this section that the eigenfunctions and eigenvalues of $\mathcal{H}^{bp}$ and $\mathcal{H}^{b\varphi}$ can be expressed by those of $\mathcal{H}^{sp}$ and $\mathcal{H}^{s\varphi}$, we may restrict ourselves to a discussion of the latter operators in the following.

VI. DISCUSSION OF $\mathcal{H}^{s\varphi}$ AND $\mathcal{H}^{sp}$

In this section we evaluate the eigenfunctions of $\mathcal{H}^{s\varphi}$, $\mathcal{H}^{sp}$ numerically and provide analytical results in the limits of large and small R_s. We first discuss bound state energies which are related to the stability properties of the 2π-Bloch wall and the nucleus. In view of statistical mechanical approximations, the scattering phase shifts of the continuum eigenfunctions are discussed. Furthermore, it is shown that the appearance of zero energy resonances in the spectrum require a subtle analysis of the applicability of analytical approximations.

A. Bound states

In the limit of large and small R_s, the eigenvalue problems of $\mathcal{H}^{s\varphi}$ and $\mathcal{H}^{sp}$ can be solved exactly:

For *large* R_s, the potentials $V_\pm(\frac{z}{\delta_s}, R_s)$ decay into two *independent* wells of the form $-2\delta_s^{-2}\mathrm{sech}^2(\frac{z}{\delta_s} \pm R_s)$ and we denote the corresponding operator by $\hat{\mathcal{H}}^s$. This limit of large R_s is sometimes also referred to as "thin-wall limit".[26] The bound states of $\mathcal{H}^{s\varphi}$ and $\mathcal{H}^{sp}$ are then given by the symmetric and antisymmetric combinations of the bound states of the single wells. For $R_s \to \infty$ we thus have $\chi_0^{s\varphi} \to \hat{\chi}_0^{s\varphi}$ and $\chi_1^{sp} \to \hat{\chi}_1^{sp}$, where

$$\hat{\chi}_0^{s\varphi}(z) \propto \mathrm{sech}\left(\frac{z}{\delta_s} + R_s\right) + \mathrm{sech}\left(\frac{z}{\delta_s} - R_s\right), \tag{6.1}$$

$$\hat{\chi}_1^{sp}(z) \propto \mathrm{sech}\left(\frac{z}{\delta_s} + R_s\right) - \mathrm{sech}\left(\frac{z}{\delta_s} - R_s\right). \tag{6.2}$$

Note that the rhs's of (6.1) and (6.2) are the exact zero energy eigenfunctions of $\mathcal{H}^{sp} - Q^{-1}$ and $\mathcal{H}^{s\varphi}$, respectively. Since for large R_s these operators differ by a term $\mathcal{O}(e^{-2R_s})$, we obtain within first-order perturbation theory

$$\hat{E}_0^{s\varphi}(R_s) \simeq \frac{(\hat{\chi}_0^{s\varphi}, \mathcal{H}^{s\varphi}\hat{\chi}_0^{s\varphi})}{(\hat{\chi}_0^{s\varphi}, \hat{\chi}_0^{s\varphi})}$$

$$= -\delta_s^{-2}\left[\frac{3}{\cosh^2 R_s} + \frac{1}{\sinh^2 R_s} \times \frac{2R_s - \sinh 2R_s}{2R_s + \sinh 2R_s}\right] \tag{6.3}$$

$$\simeq -8e^{-2R_s} \tag{6.4}$$

and

$$\hat{E}_1^{sp}(R_s) \simeq \frac{(\hat{\chi}_1^{sp}, \mathcal{H}^{sp}\hat{\chi}_1^{sp})}{(\hat{\chi}_1^{sp}, \hat{\chi}_1^{sp})}$$

$$= \delta_s^{-2}\left[\frac{3}{\sinh^2 R_s} + \frac{1}{\cosh^2 R_s} \times \frac{2R_s + \sinh 2R_s}{2R_s - \sinh 2R_s}\right] + Q^{-1} \tag{6.5}$$

$$\simeq 8e^{-2R_s} + Q^{-1}, \tag{6.6}$$

where (u, v) denotes the standard scalar product $\int dz u^* v$.

For *small* R_s, we have $\mathcal{H}^{s\varphi} \to \bar{\mathcal{H}}^{s\varphi}$ and $\mathcal{H}^{sp} \to \bar{\mathcal{H}}^{sp}$ with

$$\bar{\mathcal{H}}^{s\varphi} = -\frac{d^2}{dz^2} + \delta_s^{-2}\left[1 - 6\,\mathrm{sech}^2\left(\frac{z}{\delta_s}\right)\right], \tag{6.7}$$

$$\bar{\mathcal{H}}^{sp} = -\frac{d^2}{dz^2} + \delta_s^{-2}\left[1 - 2\,\mathrm{sech}^2\left(\frac{z}{\delta_s}\right)\right] + Q^{-1}. \tag{6.8}$$

Both potentials (6.7), (6.8) belong to the class of reflectionless potentials which are discussed in the Appendix.

The (unnormalized) bound states of $\bar{\mathcal{H}}^{s\varphi}$ and their energies are given by

$$\bar{\chi}_0^{s\varphi}(z) = \mathrm{sech}^2\frac{z}{\delta_s}, \quad \bar{E}_0^{s\varphi} = -3\delta_s^{-2}, \tag{6.9}$$

$$\bar{\chi}_1^{s\varphi}(z) = \mathrm{sech}\frac{z}{\delta_s}\tanh\frac{z}{\delta_s}, \quad \bar{E}_1^{s\varphi} = 0, \tag{6.10}$$

and the unnormalized spin-wave states read

$$\bar{\chi}_k^{s\varphi}(z) = \left(3\tanh^2\frac{z}{\delta_s} - 3ik\delta_s\tanh\frac{z}{\delta_s} - 1 - (k\delta_s)^2\right)e^{ikz}, \tag{6.11}$$

$$\bar{E}_k^{s\varphi} = \delta_s^{-2} + k^2.$$

The operator $\bar{\mathcal{H}}^{sp}$ is up to rescaling analogous to the operator (4.3) which describes the fluctuations around a single π-domain wall. It has one bound state $\bar{\chi}_0^{sp}(z) = \mathrm{sech}(z/\delta_s)$ with energy $\bar{E}_0^{sp} = Q^{-1}$, and spin-wave states

$$\bar{\chi}_k^{sp}(z) = \left(-ik\delta_s + \tanh\frac{z}{\delta_s}\right)e^{ikz},$$
$$\bar{E}_k^{sp} = Q^{-1} + \delta_s^{-2} + k^2. \tag{6.12}$$

In Eqs. (6.7)–(6.13) we have to put $\delta_s = R_s$ in order to be consistent with the terms neglected in the derivation of $\bar{\mathcal{H}}^{sp}$ and $\bar{\mathcal{H}}^{s\varphi}$.

We are now in a position to verify the asymptotic behavior of the instability threshold of the 2π-Bloch wall. Inserting (6.4), (6.9) into (5.10) we obtain (5.11), (5.12), respectively.

For arbitrary R_s, the bound state energies of $\mathcal{H}^{s\varphi}$ and $\mathcal{H}^{sp}$ have been evaluated numerically and the results are summarized in Fig. 5. The values of the asymptotic formulas (6.3) and (6.5) are represented by dashed lines. Note that they are accurate for values as small as $R_s \simeq 1.5$. The operator $\mathcal{H}^{s\varphi}$ has three bound states, the ground state of negative energy $E_0^{s\varphi}$, the zero mode

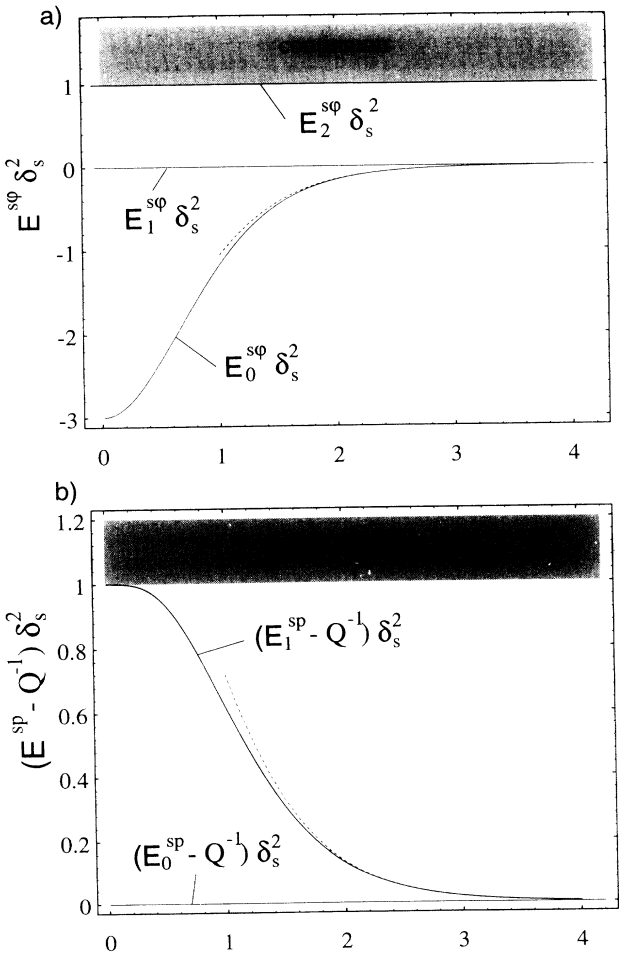

FIG. 5. The rescaled bound state energies of $\mathcal{H}^{s\varphi}$ and $\mathcal{H}^{sp}$ are shown as a function of R_s ($\delta_s = \coth R_s$). The shaded region indicates the continuum states. The horizontal lines $E_1^{s\varphi}$ and E_0^{sp} correspond to the zero modes of $\mathcal{H}^{s\varphi}$ and $\mathcal{H}^{bp}$, respectively. $E_2^{s\varphi}$ is a very weakly bound state just below the continuum threshold. The dashed lines indicate the approximation formulas (6.3) and (6.5). The bound state energies of $\mathcal{H}^{b\varphi}$ and $\mathcal{H}^{bp}$ may be obtained from (5.3),(5.4).

with $E_1^{s\varphi} = 0$, and a weakly bound state whose energy is always within 1% of the continuum threshold according to numerical calculations. For applications such as the evaluation of nucleation rates we can therefore use

$$E_2^{s\varphi} \simeq \delta_s^{-2}. \tag{6.13}$$

This bound state does not seem to be a numerical artifact since its existence also follows from the long-wavelength behavior of the scattering phase shifts $\Delta_{(e)}^{s\varphi}$ as we shall see in the next section. The ground state wave function $\chi_0^{s\varphi}$ can be considered as an internal "breathing" mode of the nucleus, corresponding to an expansion or shrinking, depending on the sign of $\chi_0^{s\varphi}$. Note, however, that according to (6.1), $\chi_0^{s\varphi} \propto d\phi_s/dR_s$ only holds in the limit $R_s \to \infty$. The operator $\mathcal{H}^{sp}$ always has two bound states. The ground state with constant energy $E_0^{sp} = Q^{-1} > 0$ has its origin in the Goldstone mode of the 2π-Bloch wall while the excited state χ_1^{sp} of energy E_1^{sp} is related to the "breathing" mode of the 2π-Bloch wall.

Comparing the previous analytical discussion with these numerical results we are left with a paradox. $\bar{\mathcal{H}}^{s\varphi}$ and $\hat{\mathcal{H}}^{s}$ both have *two* bound states, whereas numerical calculations reveal the existence of *three* bound states of $\mathcal{H}^{s\varphi}$. Similarly, $\bar{\mathcal{H}}^{sp}$ has *one* bound state, whereas $\hat{\mathcal{H}}^{s}$ and $\mathcal{H}^{sp}$ have *two* bound states. The resolution of this paradox lies in the fact that each of the operators obtained in the limits $R_s \to 0, \infty$ exhibits a zero energy bound state. Any increase in the potential strength thus leads to an additional bound state which is precisely the reason for the excess bound states of $\mathcal{H}^{s\varphi}$ and $\mathcal{H}^{sp}$. The two-well approximation $\hat{\mathcal{H}}^{s}$ has the same number of bound states as $\mathcal{H}^{sp}$ but an additional zero energy resonance. As R_s becomes finite, the zero energy resonance of $\hat{\mathcal{H}}^{s}$ is shifted into the continuum.

B. Scattering phase shifts

The knowledge of scattering phase shifts is of importance for statistical mechanical applications. In particular, the results of the present section will be used in the following paper[17] on nucleation of domain-wall pairs. The scattering phase shifts $\Delta_{(o)}^{si}$ ($\Delta_{(e)}^{si}$) of the odd (even) eigenfunctions $\chi_{k,(o)}^{si}$, ($\chi_{k,(e)}^{si}$) of the operators $\mathcal{H}^{si}$, $i = \varphi, p$ are defined as follows:

$$\chi_{k,(e)}^{si}(z \to \pm\infty, R_s) \propto \cos\left[kz \pm \Delta_{(e)}^{si}(k, R_s)/2\right], \tag{6.14}$$
$$\chi_{k,(o)}^{si}(z \to \pm\infty, R_s) \propto \sin\left[kz \pm \Delta_{(o)}^{si}(k, R_s)/2\right], \tag{6.15}$$

where $i = \varphi, p$. It is sufficient to restrict our considerations to the phase shifts of $\mathcal{H}^{s\varphi}$, since according to (5.5), (5.6) we have

$$\Delta_{(j)}^{b\varphi}(k, R) = \Delta_{(j)}^{sp}\left(\frac{\delta_b}{\delta_s}k, R\right), \tag{6.16}$$

$$\Delta_{(j)}^{bp}(k, R) = \Delta_{(j)}^{s\varphi}\left(\frac{\delta_b}{\delta_s}k, R\right), \tag{6.17}$$

where $j = e, o$.

For *large* R_s, the potentials $-2\delta_s^{-2}\mathrm{sech}^2(z/\delta_s \pm R_s)$ act as independent scattering centers, each contributing a phase shift $2\arctan(1/k\delta_s)$. Therefore we have

$$\hat{\Delta}^s(k) = 4\arctan\frac{1}{k\delta_s}. \tag{6.18}$$

For *small* R_s, the continuum eigenfunctions (6.12) and (6.13) of $\bar{\mathcal{H}}^{s\varphi}$ and $\bar{\mathcal{H}}^{sp}$ lead to[27]

$$\bar{\Delta}^{s\varphi}(k) = 2\arctan\frac{3k\delta_s}{(k\delta_s)^2 - 2}, \tag{6.19}$$

$$\bar{\Delta}^{sp}(k) = 2\arctan\frac{1}{k\delta_s}. \tag{6.20}$$

Equations (6.18)–(6.20) do not distinguish between odd- and even-parity eigenfunctions.

It is a surprising fact that some of the scattering phases $\Delta^{si}_{(j)}$, $i = \varphi, p$, $j = e, o$, *do not converge uniformly* to (6.18)–(6.20) in the limits $R_s \to 0$ and $R_s \to \infty$, respectively. Numerical calculations show that (cf. Figs. 6,7),

$$\begin{aligned}\Delta^{s\varphi}_{(e)}(k \to 0, R_s) &= 3\pi,\\ \Delta^{sp}_{(e)}(k \to 0, R_s) &= \pi,\\ \Delta^{sp}_{(o)}(k \to 0, R_s) &= 2\pi,\end{aligned} \tag{6.21}$$

for all R_s. Equations (6.18)–(6.20), however, deliver the relations

$$\begin{aligned}\bar{\Delta}^{s\varphi}(k \to 0) &= 2\pi,\\ \hat{\Delta}^s(k \to 0) &= 2\pi,\\ \bar{\Delta}^{sp}(k \to 0) &= \pi.\end{aligned} \tag{6.22}$$

This discrepancy has the same roots as the paradox encountered in the previous subsection, namely, the existence of zero energy resonances. This is elucidated by the widely unknown 1D version of Levinson's theorem[28] which relates the long-wavelength limit of the phase shifts with the number of bound states:

The *odd-parity* wave functions behave like in a 3D scattering problem:

$$\Delta^{si}_{(o)}(k \to 0) = 2\pi N^i_{(o)}, \quad i = \varphi, p, \tag{6.23}$$

where $N^i_{(o)}$ is the number of odd-parity bound states of $\mathcal{H}^{si}$. In the absence of zero energy resonances, the scattering phase shifts of *even-parity* wave functions obey a different relation

$$\Delta^{si}_{(e)}(k \to 0) = 2\pi(N^i_{(e)} - \tfrac{1}{2}), \quad i = \varphi, p, \tag{6.24}$$

where $N^i_{(e)}$ is the number of even-parity bound states of $\mathcal{H}^{si}$. According to the previous subsection, we have for all values of R_s

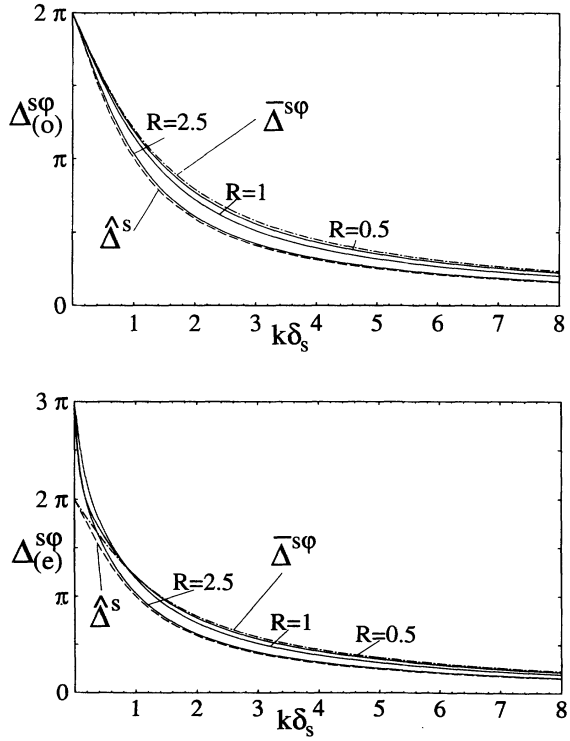

FIG. 6. The odd- and even-parity scattering phases of $\mathcal{H}^{s\varphi}$ are shown for different values of R_s ($\delta_s = \coth R_s$). $\bar{\Delta}^{s\varphi}(k)$ and $\hat{\Delta}^s(k)$ are given by (6.18)–(6.20). Note that the convergence $\Delta^{s\varphi}_{(e)}(k) \to \bar{\Delta}^{s\varphi}(k)$ for $R_s \to 0$ and $\Delta^{s\varphi}_{(e)}(k) \to \hat{\Delta}^s(k)$ for $R_s \to \infty$ is nonuniform.

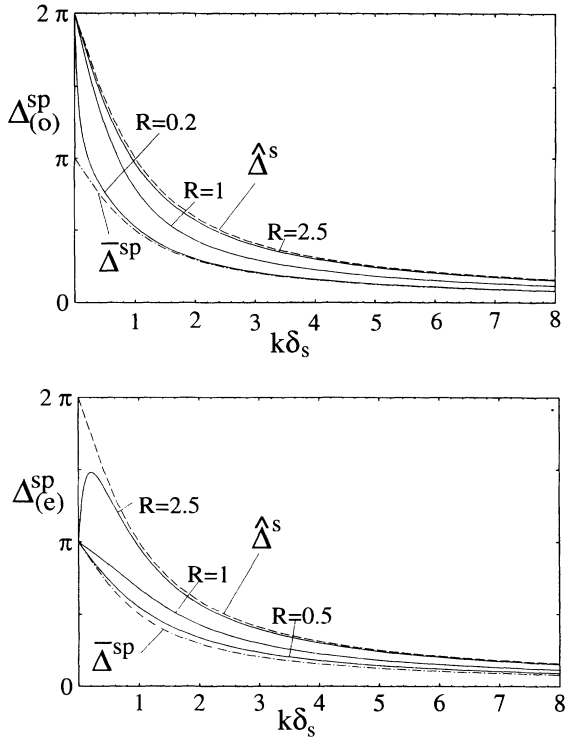

FIG. 7. The odd- and even-parity scattering phases of $\mathcal{H}^{sp}$ are shown. The convergence $\Delta^{sp}_{(o)}(k) \to \bar{\Delta}^{sp}(k)$ for $R_s \to 0$ and $\Delta^{sp}_{(e)}(k) \to \hat{\Delta}^s(k)$ for $R_s \to \infty$ is nonuniform.

$$N^{p}_{(e)} = N^{p}_{(o)} = N^{\varphi}_{(o)} = 1, \tag{6.25}$$

$$N^{\varphi}_{(e)} = 2. \tag{6.26}$$

This shows that the $k \to 0$ behavior of the scattering phase shifts (6.21) is in complete agreement with the number of bound states of $\mathcal{H}^{s\varphi}$ and $\mathcal{H}^{sp}$ as evaluated in the previous subsection.

If zero energy resonances are present and if the potential is *reflectionless*, Eqs. (6.23), (6.24) have to be replaced[28] by the *parity-independent* expression

$$\Delta^{si}_{(j)}(k \to 0) = \pi \left(N^{i}_{(e)} + N^{i}_{(o)} \right), \tag{6.27}$$

where $i = \varphi, p$ and $j = e, o$. Equation (6.27) relates (6.22) to the number of bound states of the reflectionless operators $\bar{\mathcal{H}}^{s\varphi}$, $\bar{\mathcal{H}}^{sp}$, and $\hat{\mathcal{H}}^{s}$ as given in (6.4)–(6.12). Levinson's theorem thus relates the nonuniform convergence of the scattering phase shifts towards $\bar{\Delta}^{s\varphi}$, $\bar{\Delta}^{sp}$, $\hat{\Delta}^{s}$ to the appearance of zero energy resonances in $\bar{\mathcal{H}}^{s\varphi}$, $\bar{\mathcal{H}}^{sp}$, and $\hat{\mathcal{H}}^{s}$. How this subtlety affects statistical mechanical considerations, will be discussed in the following paper.[17]

The short-wavelength behavior of the scattering phase shifts can be described within Born's approximation.[29] For an operator $-d^2/dz^2 + V(z)$ with a symmetric potential $[V(z \to \pm\infty) = 0]$, the phase shift is given by

$$\tan \frac{\Delta^{si}_{(j)}(k)}{2} \simeq -\frac{1}{2k} \int_{-\infty}^{\infty} dz\, V(z) \sin^2(kz). \tag{6.28}$$

If k^{-1} is much smaller than variations in $V(z)$, we can use $\sin^2(kz) \simeq 1/2$ and after insertion of $V_{\pm}(z/\delta_s, R_s) - \delta_s^{-2}$ [cf. (4.13)] into (6.28) we obtain

$$\frac{\Delta^{si}_{(j)}(k)}{2} \simeq \frac{1}{k\delta_s} \left[2 \mp \frac{R_s}{\sinh R_s \cosh R_s} \right] \quad \text{for } k\delta_s \gg 1, \tag{6.29}$$

where the upper sign refers to the $i = p$ and the tan function has been replaced by its argument. Finally it is interesting to note that for $\bar{\mathcal{H}}^{sp}$ the Born approximation (6.28) with $\sin^2(kz) \to 1/2$ coincides with the exact result (6.20).

VII. 2π-BLOCH WALLS IN THIN FILMS

The results of the previous sections are rigorous within the 1D model of a biaxial ferromagnet which contains exchange and local anisotropies and the coupling to an external field. While we have seen in Sec. II that local demagnetizing effects can be incorporated into the model by a redefinition of the anisotropy constants, one might question the applicability to thin films where nonlocal demagnetizing effects are not *a priori* negligible. Since the nonlocal demagnetizing interaction decays algebraically while the exchange interaction between domain walls decreases exponentially, we expect the exchange interaction to be dominant and thus our model to be adequate for small domain-wall separations.

Indeed, it is the purpose of this section to show that for sufficiently thin films and at external fields below the threshold (5.10), twisted domain-wall pairs may be brought sufficiently close such that the exchange interaction between the individual domain walls becomes important and nonlocal demagnetizing effects become irrelevant. In this case our model adequately describes the equilibrium separation of the walls. We shall use cgs units throughout this section.

To be specific, we choose coordinate axes as in Figs. 8(a), and 8(b) and consider a film of thickness D in the x direction which extends infinitely in the y direction and has length L in the z direction. Further we assume the magnetization to be strictly one dimensional, i.e., $\mathbf{M} = \mathbf{M}(z)$. The demagnetizing energy per area, $\mathcal{E}_m = -(1/2D) \int dx\, dz\, \mathbf{H}_m(x,z) \cdot \mathbf{M}(z)$, can then be cast into a very convenient form due to Dietze and Thomas:[32]

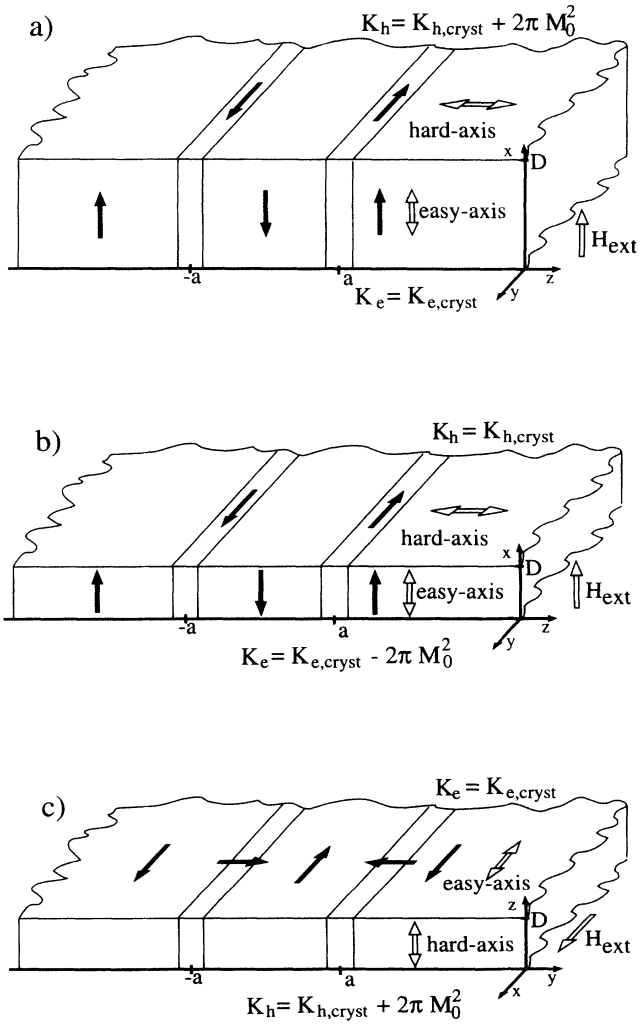

FIG. 8. Magnetization configurations in films that can be described by the model (2.8). Note that the anisotropy constant has to be chosen as indicated to incorporate the local part of the magnetostatic interaction. Note also that the orientation of the coordinate frame in (a) as used in the text is different from (b) and (c).

$$\mathcal{E}_m = \int_{-L/2}^{L/2} dz\, 2\pi M_z^2(z) + \frac{1}{D}\int_{-L/2}^{L/2} dz \int_{-L/2}^{L/2} dz' \,[M_x(z)M_x(z') - M_z(z)M_z(z')] \times \ln\left(1 + \frac{D^2}{(z-z')^2}\right). \tag{7.1}$$

Equation (7.1) reduces to a simple hard-axis anisotropy energy in the following two limiting cases:

For a film thickness D smaller than the characteristic length scale of $\mathbf{M}$, i.e., smaller than the domain-wall width, the integration over the relative coordinate in the second term on the rhs in (7.1) can be performed, and Eq. (7.1) reduces to

$$\mathcal{E}_m = 2\pi \int_{-L/2}^{L/2} dz\, M_x^2(z). \tag{7.2}$$

This has the form of a hard-axis anisotropy energy normal to the film plane.

In the opposite limit of large $D \gg L$, the second term on the rhs of (7.1) tends to zero[30] and we recover the result (2.4). This form of the demagnetizing energy is used for the description of domain-wall dynamics in moderately thin ($\simeq$ 1 μm) rare earth garnet films.[1,2]

As the magnetostatic interaction has the form of a hard-axis anisotropy in these limits, the energy density (2.8) can be used to describe three distinct experimental configurations. In addition to the bulk situation considered so far [cf. Fig. 8(a)], it describes configurations in thin films ($D/\sqrt{A/K_e} \leq 1$) which are perpendicularly [Fig. 8(b)] or in-plane [Fig. 8(c)] magnetized provided that the coordinate axes are chosen appropriately. The results of the previous sections thus hold for all configurations shown in Fig. 8 in the limit of infinitesimally thin films. In the following it is discussed how *nonlocal demagnetizing fields*, i.e., the nonlocal contribution in (7.1), will affect these results for a film of finite thickness.

A. Perpendicularly magnetized films

Consider a situation as in Fig. 8(b) which requires the crystalline easy-axis anisotropy to be larger than the demagnetizing energy, i.e., $K_{e,\text{cryst}} > 2\pi M_0^2$, and the easy axis to be oriented perpendicularly to the film, a situation typically realized in bubble films or in barium-ferrite. To estimate the nonlocal demagnetizing interaction for domain-wall separations large compared to a domain-wall width, we consider the configuration

$$\mathbf{M}^{(0)}(\mathbf{r}) = \begin{cases} M_0\mathbf{e}_x & \text{for } L > |z| > a, \\ -M_0\mathbf{e}_x & \text{for } |z| \leq a, \end{cases} \tag{7.3}$$

for $0 \leq x \leq D$, $-\infty < y < \infty$, and vanishing elsewhere. The nonlocal magnetostatic interaction is due to the nonuniform surface charge distribution caused by the reversed domain at $|z| \leq a$ [cf. Fig. 8(b)]. Inserting (7.3) into (7.1) and performing the limit $L \to \infty$ *after* evaluation of the integrals, we obtain[31]

$$\mathcal{E}_m^{\text{perp}} = \mathcal{E}_m[\mathbf{M}^{(0)}] - \mathcal{E}_m[M_0\mathbf{e}_x] = -4M_0^2 D\alpha\left\{4\tan^{-1}\frac{1}{\alpha} + 2\alpha\ln\alpha + \left(\frac{1}{\alpha} - \alpha\right)\ln(1+\alpha^2)\right\}, \tag{7.4}$$

where $\alpha = 2a/D$ is the width of the reversed domain with respect to the film thickness. Note that the rhs of (7.4) decreases with increasing α and thus favors an expansion of the reversed domain independent of the relative twist of the domain walls. For the twisted domain-wall pair it thus competes with the repulsive exchange interaction.

An external magnetic field H_{ext} along the positive x direction [cf. Fig. 8(b)] will counteract this magnetostatic repulsion. A relation for the corresponding equilibrium width is obtained by minimizing the energy (7.4) plus the Zeeman energy of the intermediate domain, $2M_0H_{\text{ext}}D\alpha$, with respect to α with the result

$$\frac{H_{\text{ext}}}{4\pi M_0} = \frac{2}{\pi}\tan^{-1}\frac{1}{\alpha} - \frac{\alpha}{\pi}\ln\left(1 + \frac{1}{\alpha^2}\right). \tag{7.5}$$

Note that the relation (7.5) does not depend on the absolute size of the reversed domain but only on its relative size with respect to the film thickness. Since on the other hand the mutual exchange repulsion of twisted domain walls depends on their absolute distance, it can only be observed if the equilibrium width in Eq. (7.5) is small. However, since the external field must not exceed the instability threshold, this can only be achieved in sufficiently thin films.

To investigate this effect quantitatively, we have to compare the equilibrium width $2a = \alpha D$ of (7.5) with the separation $2a = 2R_b\delta_b\delta_0$ of the domain walls forming a 2π-Bloch wall (3.16), (3.17) where $\delta_0 = \sqrt{A/K_e}$ is the static Bloch-wall width. It is sufficient to look at small $H_{\text{ext}}M_0/(2K_e)$ where this relation between equilibrium width and external field can be expressed as

$$\frac{H_{\text{ext}}}{4\pi M_0} = \frac{2K_e}{\pi M_0^2}\exp\left\{-\frac{2a}{\delta_0}\right\}. \tag{7.6}$$

This topological (exchange) interaction between the domain walls thus decreases exponentially, while the magnetostatic interaction (7.5) decays algebraically, i.e., $H_{\text{ext}}/4\pi M_0 = D/(2\pi a)$, for large $2a/D$. Since the rhs of (7.6) is proportional to the "quality factor" $K_e/(2\pi M_0^2)$ of the domain-wall, the exchange repulsion will manifest itself at larger domain wall separations with increasing quality factors and decreasing film thickness.

This is illustrated in Fig. 9 where the solid lines show the exchange dominated-wall separation (7.6) whereas the dashed lines represent (7.5). The experimentally required field to reach a certain wall separation will follow the curve that has the maximal value of H_{ext} consistent with the sample parameters. Note that the exchange repulsion between the domain walls has a drastic effect. E.g., for a film with $D/\delta_0 = 0.1$ and $K_e/(2\pi M_0^2) = 10$, the external fields to establish a distance of $7\delta_0$ predicted by (7.6) exceed that of (7.5) by an order of magnitude

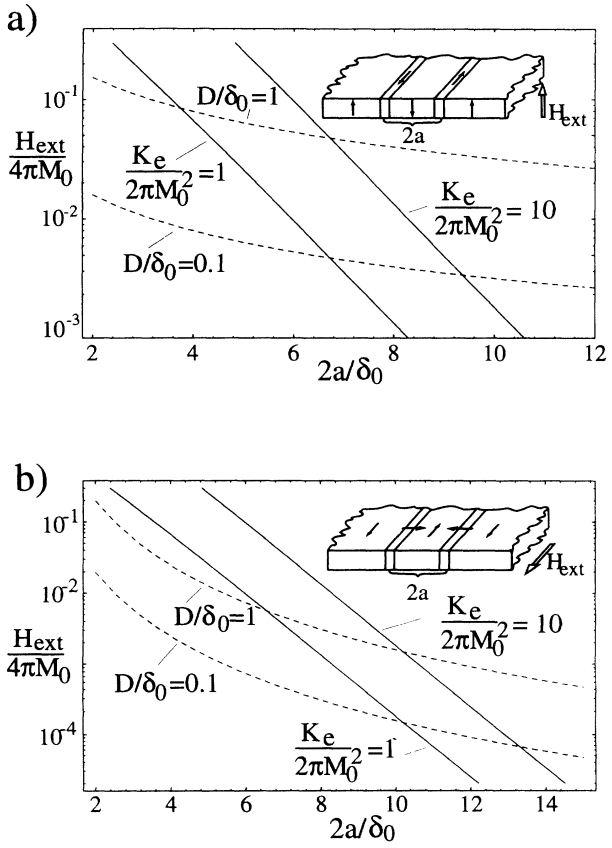

FIG. 9. Domain-wall separations for a twisted domain-wall pair in (a) perpendicularly and (b) in-plane magnetized films due to balance between external field and exchange [solid line, Eq. (7.6)] or between external field and demagnetizing effects [dashed line, (a) Eq. (7.5), (b) Eq. (7.8)].

or, vice versa, the wall separations differ by a factor of 3 for $H_{ext}/(4\pi M_0) = 0.01$. This large discrepancy should be accessible to experimental verification.

So far we did not discuss the case of untwisted domain-wall pairs. Despite the fact that they have been shown to be unstable in Sec. V, Eq. (7.5) shows that such domain-wall pairs can exist in thin films due to the balance of demagnetizing and Zeeman energy, provided they are well separated. However, the ansatz (7.3) overestimates demagnetizing effects. As the wall separation decreases, the untwisted walls annihilate each other [cf. Fig. 2(a)] and the magnetostatic surface charges are drastically reduced compared to those of (7.3). This implies that the experimentally observed separation of untwisted wall pairs will not follow the dashed curve in Fig. 9 down to vanishing a but exhibit an instability at finite a. This instability will occur at fields that are much smaller than the instability threshold of the twisted domain-wall pair. We do not consider this case further but conclude with the remark that a quantitative theory can be obtained by improving the ansatz (7.3) by replacing it by the nucleus solution (ϕ_s, θ_s).

B. In-plane magnetized films

Consider the configuration shown in Fig. 8(c) with a crystalline easy axis in the film plane. All previous formulas hold also for this configuration provided that we redefine all coordinates appropriately, i.e., $(x, y, z) \to (z, x, y)$. Since the magnetization configuration is exclusively in the film plane, there are no induced magnetostatic surface charges in a film that extends infinitely in the x direction and there is no equilibrium domain formation in the infinite film geometry. However, we assume that domain walls exist that have been created, e.g., by nucleation at a sample end and/or nonuniform external fields. If domain walls are present, a magnetostatic interaction arises between the magnetostatic volume charges of the domain walls. For sufficiently well separated twisted domain wall pairs, Eq. (3.17) takes the form $M_y/M_0 = \mathrm{sech}[(y+a)/\delta_0] - \mathrm{sech}[(y-a)/\delta_0]$. Inserting this into (7.1) (with redefined coordinate axes) we obtain, for a much larger than a domain-wall width δ_0,

$$\mathcal{E}_m^{\mathrm{ip}} = 2D(\pi M_0)^2 \left(\frac{\delta_0}{2a}\right)^2 . \tag{7.7}$$

Equation (7.7) is simply the interaction energy of two infinitely long strings of dipoles along y with dipole moment per unit length, $\mu_y = D\int dy M_y(y) = D\delta_0 \pi M_0$. The magnetostatic interaction between the walls is thus repulsive for the twisted domain-wall pair and competes with the exchange interaction between the individual walls. (For untwisted domain-wall pairs the magnetostatic as well as the exchange interaction would be attractive.) An external magnetic field in the x direction will counteract this repulsion. The equilibrium distance $2a$ between two domain walls is obtained by minimization of demagnetizing plus Zeeman energy, $\mathcal{E}_m^{\mathrm{ip}} + 4M_0 H_{\mathrm{ext}} a$, with the result

$$\frac{H_{\mathrm{ext}}}{4\pi M_0} = \frac{\pi}{2}\frac{D}{\delta_0}\left(\frac{\delta_0}{2a}\right)^3 . \tag{7.8}$$

In Fig. 9(b), this is compared with the wall separation (7.6) which is predicted by our model. Demagnetizing effects are obviously weaker than in a perpendicularly magnetized film. For films of thickness $D = 0.1\delta_0$ and $K_e/(2\pi M_0^2) = 10$, the exchange interaction dominates the demagnetizing interaction already at a domain-wall separation of $2a = 13\delta_0$ which is surprisingly large considering the exponential decrease of the exchange interaction (7.6). Note also that the external fields which are required to achieve a domain-wall distance of $6\delta_0$ differ by a factor of 100. Finally, we note that untwisted wall pairs in in-plane magnetized films are never stable for the anisotropy configuration shown in Fig. 8(c).

VIII. CONCLUSION

In this paper we have discussed the stability of twisted and untwisted domain-wall pairs within a 1D model of a ferromagnet. The fluctuations around these structures

have been shown to be described by the same operators. By means of exactly known eigenfunctions which are related to the Goldstone modes of these structures it has been shown that untwisted domain-wall pairs exhibit exactly one unstable mode while twisted domain-wall pairs are subject to an instability at large external fields.

Furthermore, we have argued that this model adequately describes the separation of twisted domain walls in ultrathin films and thus the above instability should be observable.

Although untwisted domain walls are unstable within the biaxial ferromagnet, they can exist in thin films at large separations due to the long-range magnetostatic interaction. However, as a consequence of their topological instability, the corresponding collapse field will be much smaller than that of twisted domain-wall pairs. There are experimental[14] and numerical[15] hints for this behavior, but more systematic studies are required to allow for a quantitative comparison with the present theory.

Another important aspect is the role of untwisted domain-wall pairs as nuclei for magnetization reversal in elongated particles. As has been reported elsewhere,[16] the existence of such nonuniform nuclei fact can lead to a substantial reduction of the coercivity compared to standard theories of magnetization reversal. Further details of the statistical mechanical theory of magnetization reversal are covered in the following paper.[17]

ACKNOWLEDGMENTS

I kindly acknowledge illuminating discussions with W. Baltensperger, O. Brodbeck, J.S. Broz, J. Hołyst, S. Skourtis, and H. Suhl. This work has been supported by the Swiss National Science Foundation and by ONR Grant No. N00014-90-J-1202.

APPENDIX

In (4.3), (6.7), (6.8) we encountered Schrödinger operators of the form

$$\mathcal{H}^{(m)} = -\frac{d^2}{dx^2} - \frac{m(m+1)}{\cosh^2 x}, \tag{A1}$$

with m an integer. In the following, we shall show how the corresponding eigenvalue problems may be solved exactly with the method of Ref. 33. The continuum eigenfunctions of $\mathcal{H}^{(m)}$ have the remarkable property that their reflection coefficient is zero. We write the eigenvalue problem of (A1) as follows:

$$\mathcal{H}^{(m)}\psi_\lambda^{(m)} = \lambda\psi_\lambda^{(m)}. \tag{A2}$$

The key point for the solution of the eigenvalue problem (A2) is the observation that $\mathcal{H}^{(m)}$ may be factorized in two different ways:

$$\mathcal{H}^{(m)} = \mathcal{Q}_+^{(m)}\mathcal{Q}_-^{(m)} - m^2 \tag{A3}$$

$$= \mathcal{Q}_-^{(m+1)}\mathcal{Q}_+^{(m+1)} - (m+1)^2, \tag{A4}$$

with

$$\mathcal{Q}_\pm^{(m)} = \mp\frac{d}{dx} + m\tanh x. \tag{A5}$$

Operating on (A2) from the left with $\mathcal{Q}_-^{(m)}$, $\mathcal{Q}_+^{(m+1)}$, we recognize that if $\psi_\lambda^{(m)}$ is an eigenfunction of $\mathcal{H}^{(m)}$ with eigenvalue λ, then

$$\psi_\lambda^{(m-1)} = \mathcal{Q}_-^{(m)}\psi_\lambda^{(m)}, \tag{A6}$$

$$\psi_\lambda^{(m+1)} = \mathcal{Q}_+^{(m+1)}\psi_\lambda^{(m)} \tag{A7}$$

are eigenfunctions of $\mathcal{H}^{(m-1)}$, $\mathcal{H}^{(m+1)}$, respectively, to the *same* eigenvalue λ.

The *continuum eigenfunctions* of $\mathcal{H}^{(m)}$ can thus be related to those of $\mathcal{H}^{(m-1)}$. Since $\mathcal{H}^{(0)}$ represents the free problem, the continuum eigenfunctions of $\mathcal{H}^{(m)}$ can be obtained by successive application of $\mathcal{Q}_+^{(m)}$ onto plane wave solutions, i.e.,

$$\psi_k^{(m)} = \mathcal{Q}_+^{(m)}\cdots\mathcal{Q}_+^{(2)}\mathcal{Q}_+^{(1)}e^{ikx}, \tag{A8}$$

and belong to the eigenvalue $\lambda = k^2$. For $\mathcal{H}^{(1)} = -d^2/dx^2 - 2\,\mathrm{sech}^2 x$, Eq. (A8) yields

$$\psi_k^{(1)} = \mathcal{Q}_+^{(1)}e^{ikx} = [-ik + \tanh x]e^{ikx}. \tag{A9}$$

For $\mathcal{H}^{(2)} = -d^2/dx^2 - 6\,\mathrm{sech}^2 x$ we obtain the continuum eigenfunctions

$$\psi_k^{(2)} = \mathcal{Q}_+^{(2)}\mathcal{Q}_+^{(1)}e^{ikx} \tag{A10}$$

$$= [3\tanh^2 x - 3ik\tanh x - 1 - k^2]e^{ikx}. \tag{A11}$$

To find the *bound states* with $\lambda < 0$, we first remark that the normalizations of bound state eigenfunctions with different m are related as

$$\int_{-\infty}^{+\infty} dx(\psi_\lambda^{(m-1)})^2 = \int_{-\infty}^{+\infty} dx\psi_\lambda^{(m)}\mathcal{Q}_+^{(m)}\mathcal{Q}_-^{(m)}\psi_\lambda^{(m)}$$

$$= (\lambda + m^2)\int_{-\infty}^{+\infty} dx(\psi_\lambda^{(m)})^2. \tag{A12}$$

Continuing this recursion towards lower values of m we recognize that the normalization of, say, $\psi_\lambda^{(l-1)}$ would become negative. This can only be avoided if the recursion (A12) stops, i.e., if the bound state eigenvalues are given by

$$\lambda_l = -l^2, \qquad l = 1, 2, \ldots, m. \tag{A13}$$

According to (A12) this implies that

$$\mathcal{Q}_-^{(l)}\psi_{\lambda_l}^{(l)} = 0. \tag{A14}$$

This differential equation can be integrated with (A5),

$$\psi_{\lambda_l}(x) = \mathrm{sech}^l x. \tag{A15}$$

For $m > l$, the unnormalized lth bound state (counted from the continuum) can be obtained recursively with the help of (A7),

$$\psi_\lambda^{(m)} = \mathcal{Q}_+^{(m)}\cdots\mathcal{Q}_+^{(l+1)}\mathrm{sech}^l x. \tag{A16}$$

Specifically, we obtain for $m = 1$

$$\psi_1^{(1)} = \operatorname{sech} x, \tag{A17}$$

with energy $\lambda_1 = -1$, and for $m = 2$

$$\psi_2^{(2)} = \operatorname{sech}^2 x, \tag{A18}$$

$$\psi_1^{(2)} = \operatorname{sech} x \tanh x, \tag{A19}$$

with energies $\lambda_2 = -4$ and $\lambda_1 = -1$. All operators (A1) share the property of having a zero energy resonance. This means that an infinitesimal increase in the potential strength of (A1) leads to an additional bound state. Therefore, the occurrence of the operators (A1) as describing fluctuations around nonlinear structures in some limit of the external field has to be handled with care, since their number of bound states in general differs from those of the operators they emerge from.

* Present address; electronic address: hbraun@sfu.ca

[1] F.H. Leeuw, R. van den Doel, and U. Enz, Rep. Prog. Phys. **43**, 690 (1980).

[2] A.P Malozemoff and J.C. Slonczewski, *Magnetic Domain Walls in Bubble Materials* (Academic, New York, 1979).

[3] E. Koester and T.C. Arnoldussen, *Magnetic Recording* (McGraw-Hill, New York, 1987), Vol. 1, Chap. 3.

[4] See e.g., R. Rajaraman, *Solitons and Instantons* (North-Holland, Amsterdam, 1982).

[5] R. Hoogerbeets, S.A.J. Wiegers, A.J. van Duyneveldt, R.D. Willett, and U. Geisen, Physica **125B**, 135 (1984).

[6] For a review of theoretical and experimental work on effectively 1D ferromagnets and antiferromagnets, see H.-J. Mikeska and M. Steiner, Adv. Phys. **40**, 191 (1991).

[7] E.K. Sklyanin (unpublished).

[8] H.B. Braun and O. Brodbeck, Phys. Rev. Lett. **70**, 3335 (1993).

[9] F. Bloch, Z. Phys. **74**, 295 (1932).

[10] L. Landau and E. Lifshitz, Phys. Z. Sowjetunion **8**, 153 (1935).

[11] J.M. Winter, Phys. Rev **124**, 452 (1962).

[12] J.F. Janak, Phys. Rev. **134**, A411 (1964).

[13] R.M. Hornreich and H. Thomas, Phys. Rev. B **17**, 1406 (1978).

[14] L.J. Heydermann, H. Niedoba, H.O. Gupta, and I.B. Puchalska, J. Magn. Magn. Mater. **96**, 125 (1991); I. Puchalska and H. Niedoba, IEEE Trans. Magn. **MAG-27**, 3579 (1991).

[15] G.N. Patterson, R.C. Giles, and F.B. Humphrey, IEEE Trans. Magn. **MAG-28**, 2341 (1992).

[16] H.B. Braun, Phys. Rev. Lett. **71**, 3557 (1993).

[17] H.B. Braun, following paper, Phys. Rev. B **50**, 16 501 (1994).

[18] E. Magyari and H. Thomas, Phys. Scr. T **44**, 45 (1992).

[19] H.B. Braun, Ph.D. thesis, ETH Zürich, 1991.

[20] See, e.g., R.R. Katti, J.A. Dooley, and A. Meng, IEEE Trans. Magn.**MAG-29**, 2578 (1993).

[21] Neglecting magnetostatic surface charges corresponds to an infinite sample where the limits in transversal directions are performed before the one along the magnetic chain.

[22] J.S. Broz, H.B. Braun, O. Brodbeck, W. Baltensperger, and J.S. Helman, Phys. Rev. Lett. **65**, 787 (1990).

[23] K.A. Long and A.R. Bishop, J. Phys A **12**, 1325 (1979).

[24] D.K. Campbell, M. Peyrard, and P. Sodano, Physica D **19**, 165 (1986).

[25] P. Sodano, M. El-Batanouny, and C.R. Willis, Phys. Rev. B **34**, 4936 (1986).

[26] S. Coleman, Phys. Rev. D **15**, 2929 (1977).

[27] The branch of arctan is always chosen such that $\Delta(k \to \infty) = 0$ and such that $\Delta(k)$ is a continuous function.

[28] G. Barton, J. Phys. A **18**, 479 (1985).

[29] C.J. Joachain, *Quantum Collision Theory* North-Holland, Amsterdam, 1975).

[30] This can be seen with the use of the inequality $|M_x(z)M_x(z') - M_z(z)M_z(z')| \leq 2M_0^2$ and subsequent integration.

[31] Equation (7.4) is identical with a result obtained by K. Babcock and R. Westervelt, Phys. Rev. A **40**, 2022 (1989), which, however, has been derived in different way.

[32] H.D. Dietze and H. Thomas, Z. Phys. **163**, 523 (1961).

[33] L. Infeld and T.E. Hull, Rev. Mod. Phys. **23**, 21 (1951).

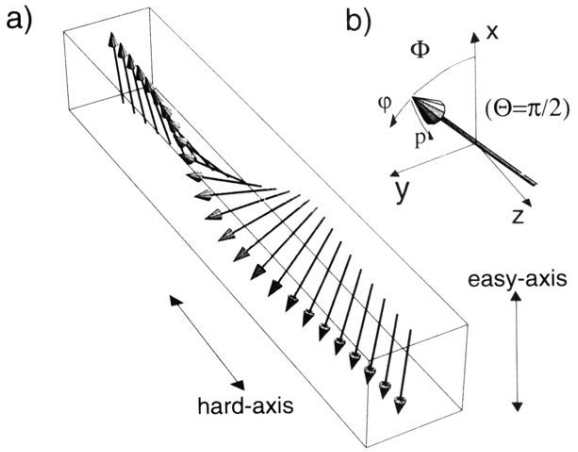

FIG. 1. (a) The π-Bloch wall interpolates between different anisotropy minima; (b) fluctuations φ, p around a given structure with ϕ_s, ϕ_b and $\theta = \pi/2$ at a given space point z.

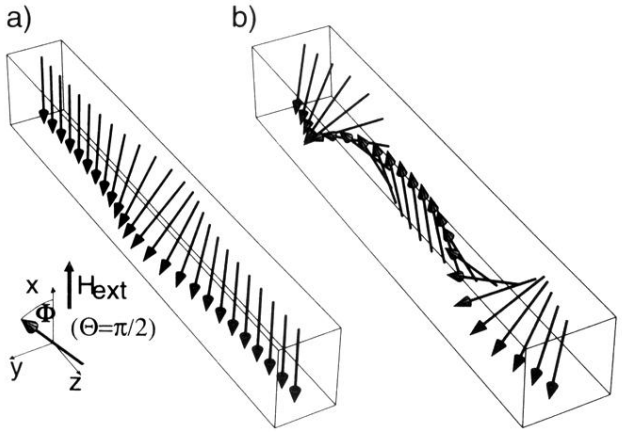

FIG. 2. The nucleus is shown for (a) small fields ($R_s = 3.5$) and (b) for fields close to the anisotropy field ($R_s = 0.4$)

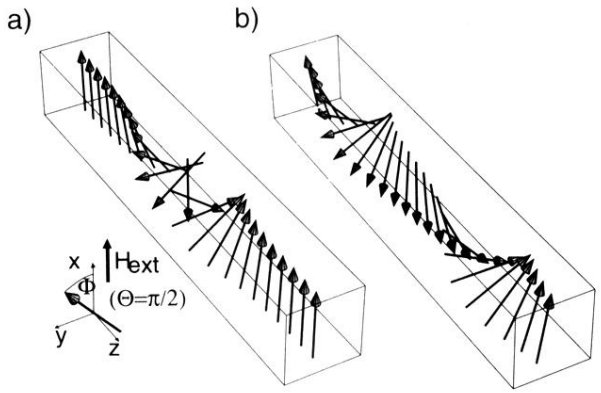

FIG. 3. The 2π-Bloch wall is shown for (a) small fields ($R_b = 3.5$) and (b) for large fields ($R_b = 0.4$)

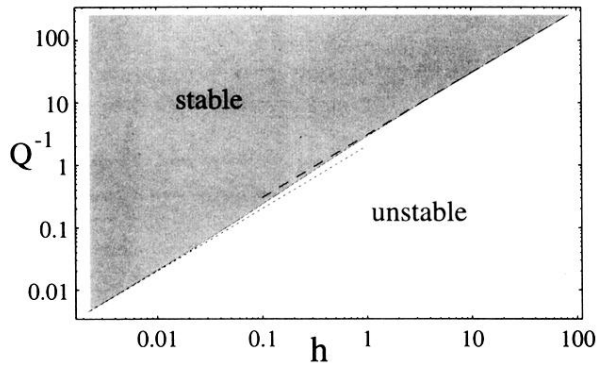

FIG. 4. Stability and instability regions of the 2π-Bloch wall as a function of the external field h and the demagnetizing field strength Q^{-1}. The dotted and dashed lines refer to (5.11) and (5.12), respectively.

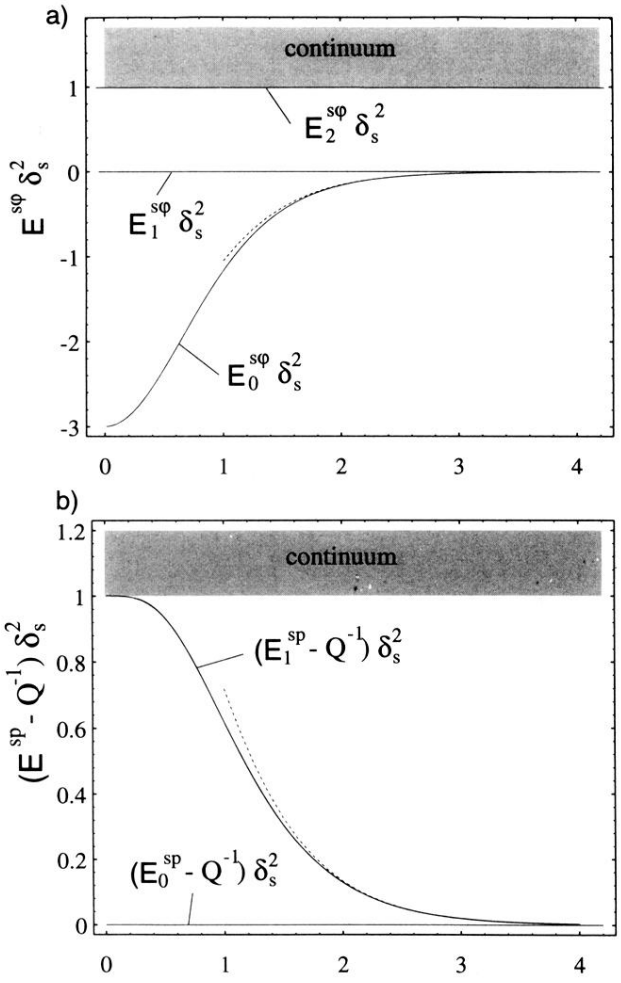

FIG. 5. The rescaled bound state energies of $\mathcal{H}^{s\varphi}$ and $\mathcal{H}^{sp}$ are shown as a function of R_s ($\delta_s = \coth R_s$). The shaded region indicates the continuum states. The horizontal lines $E_1^{s\varphi}$ and E_0^{sp} correspond to the zero modes of $\mathcal{H}^{s\varphi}$ and $\mathcal{H}^{bp}$, respectively. $E_2^{s\varphi}$ is a very weakly bound state just below the continuum threshold. The dashed lines indicate the approximation formulas (6.3) and (6.5). The bound state energies of $\mathcal{H}^{b\varphi}$ and $\mathcal{H}^{bp}$ may be obtained from (5.3),(5.4).